Supporting Information

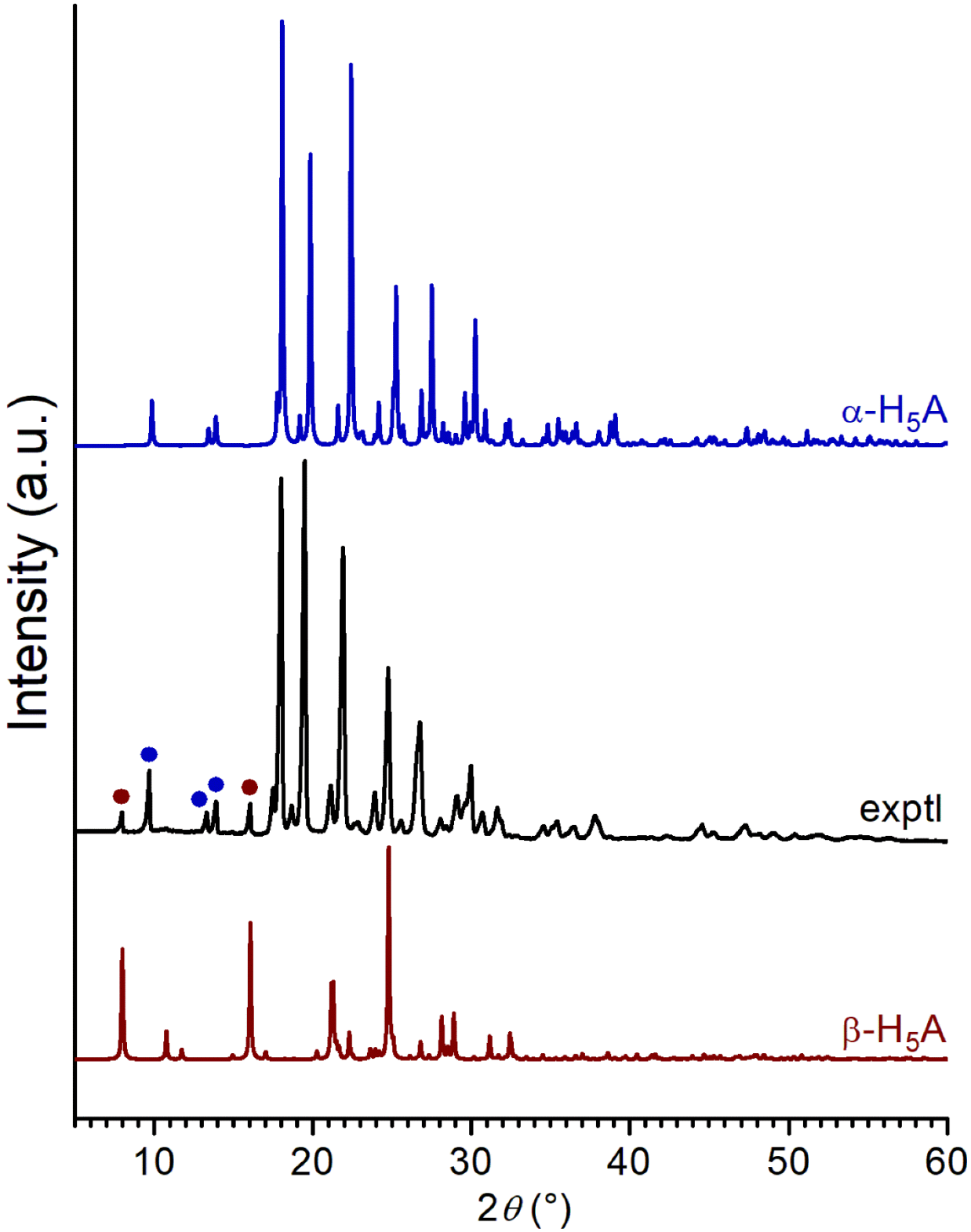

Figure S1. X-ray powder diffractogram of H_5A at room temperature. The diffraction patterns for α- and β-H_5A, calculated from single-crystal X-ray data collected at 100 and 298 K, respectively, are also shown for comparison. The high-angle shift of calculated peak positions for α-H_5A is due to low-temperature lattice contraction. The blue and wine dots mark low-angle peaks arising from the two polymorphs.

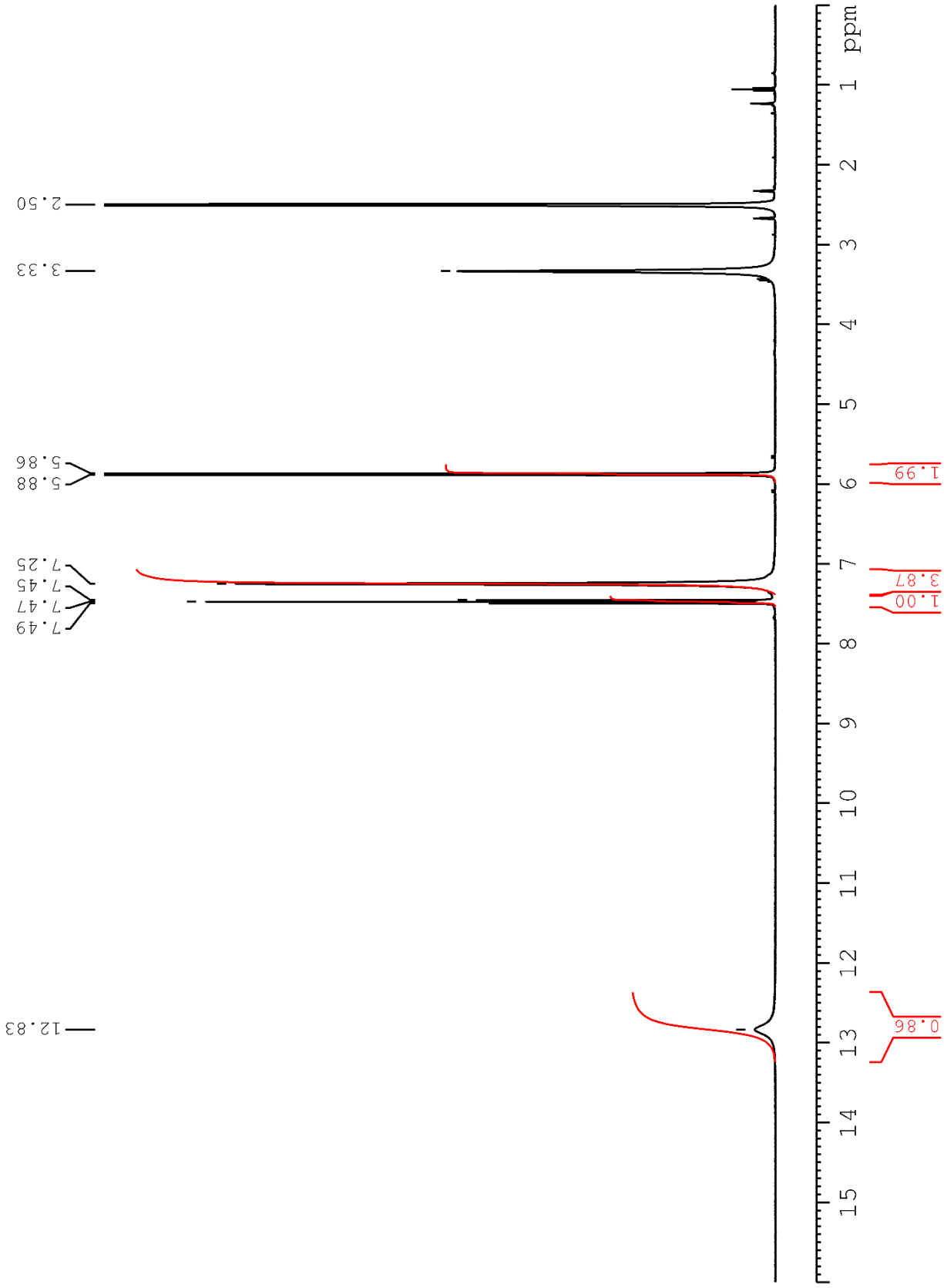

Figure S2. ^{1}H NMR spectrum of dap·HCl in $(CD_3)_2SO$ (400.13 MHz) at 298 K.

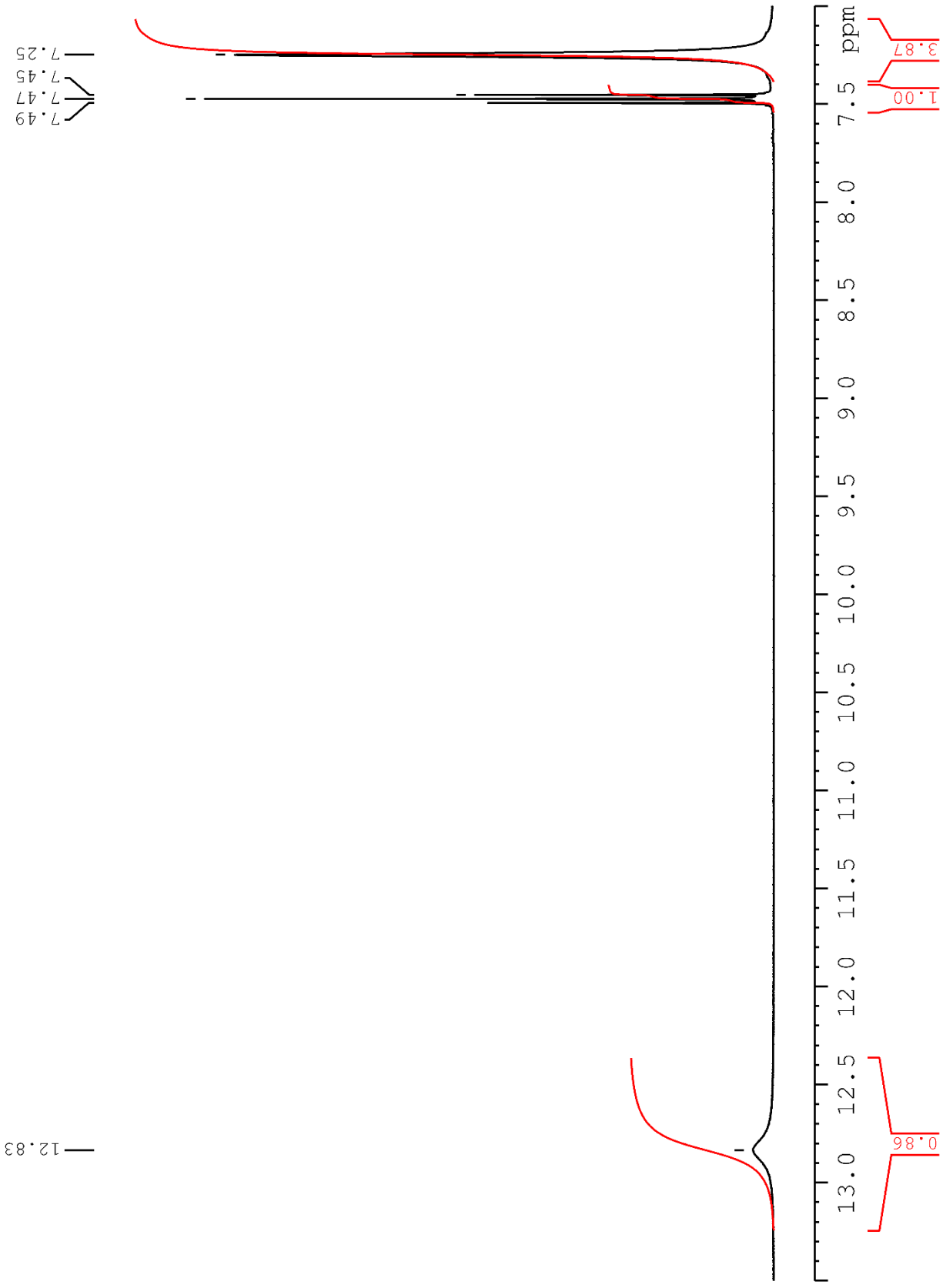

Figure S3. ^{1}H NMR spectrum of dap·HCl in $(CD_3)_2SO$ (400.13 MHz) at 298 K (expanded region).

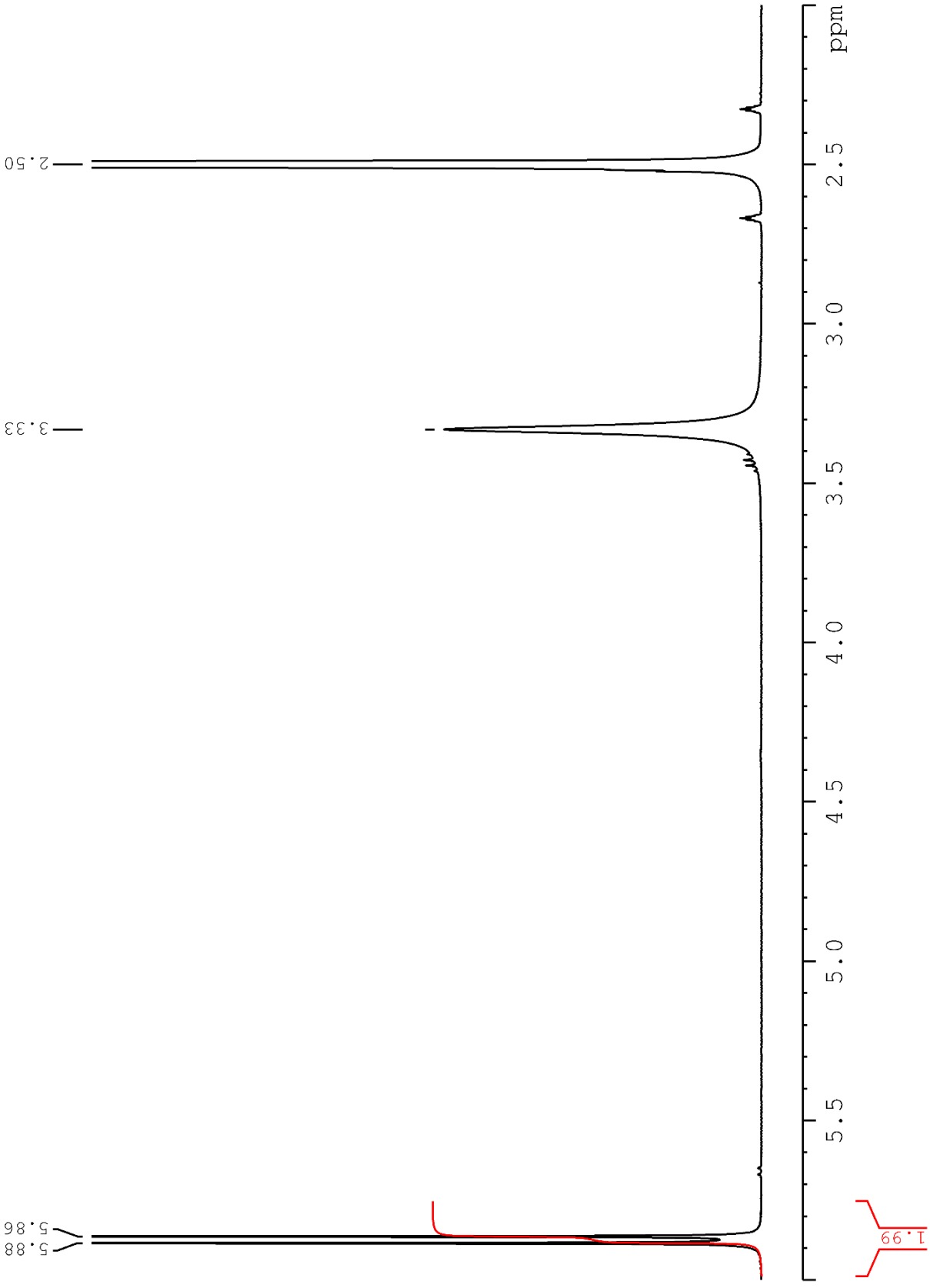

Figure S4. ^{1}H NMR spectrum of dap·HCl in $(CD_3)_2SO$ (400.13 MHz) at 298 K (expanded region).

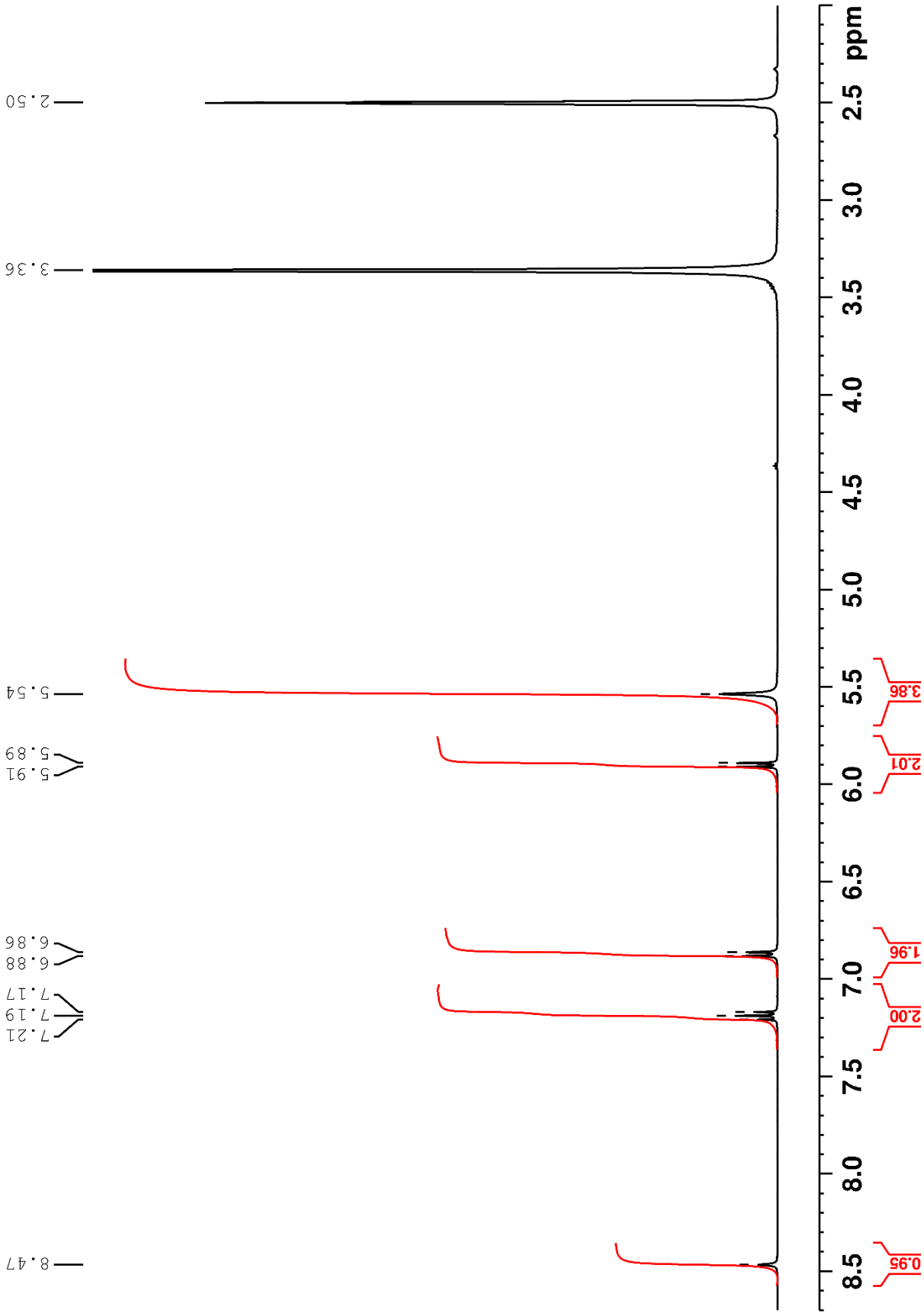

Figure S5. ^{1}H NMR spectrum of H_5A in $(CD_3)_2SO$ (400.13 MHz) at 298 K.

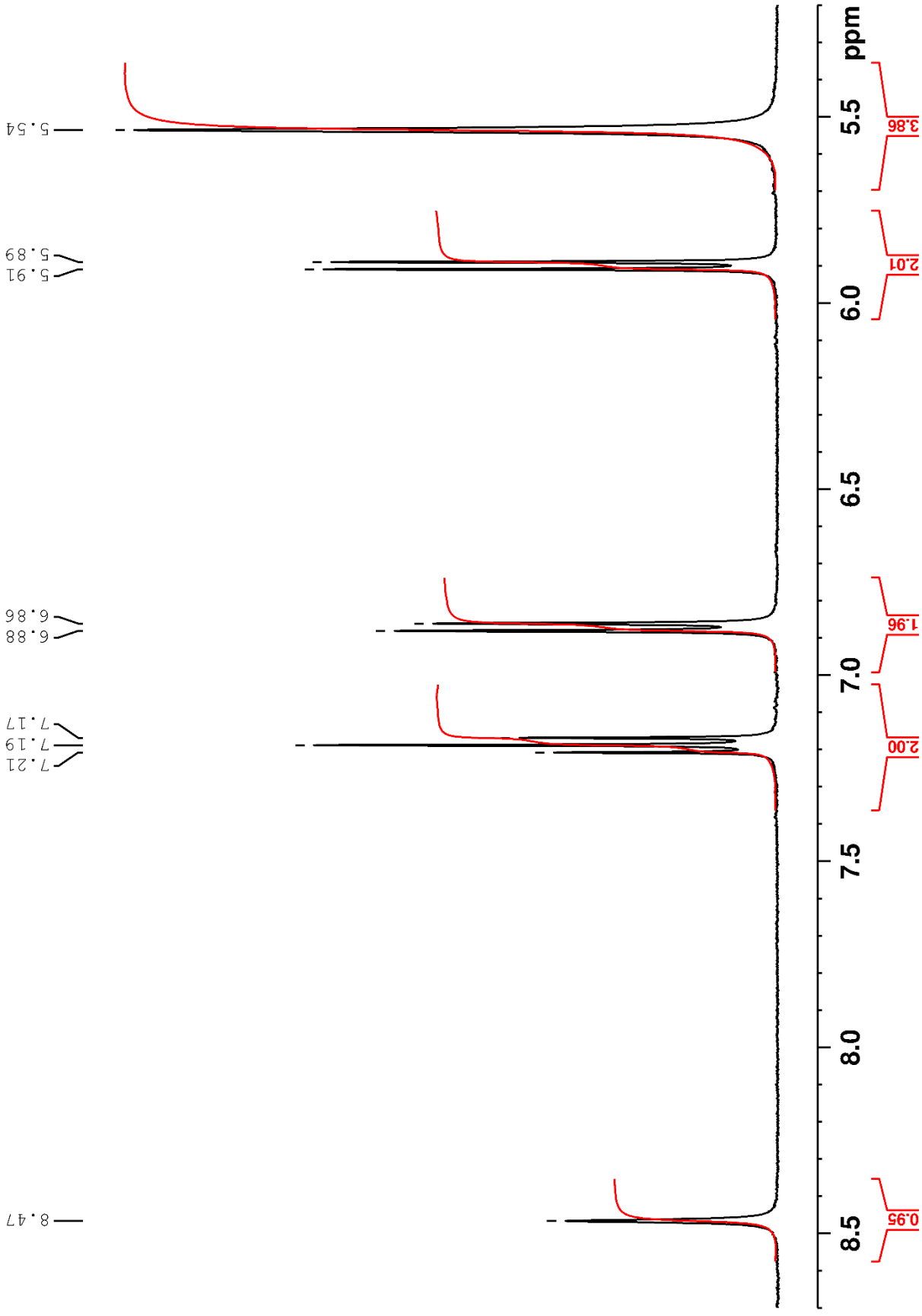

Figure S6. ^{1}H NMR spectrum of H_5A in $(CD_3)_2SO$ (400.13 MHz) at 298 K (expanded region).

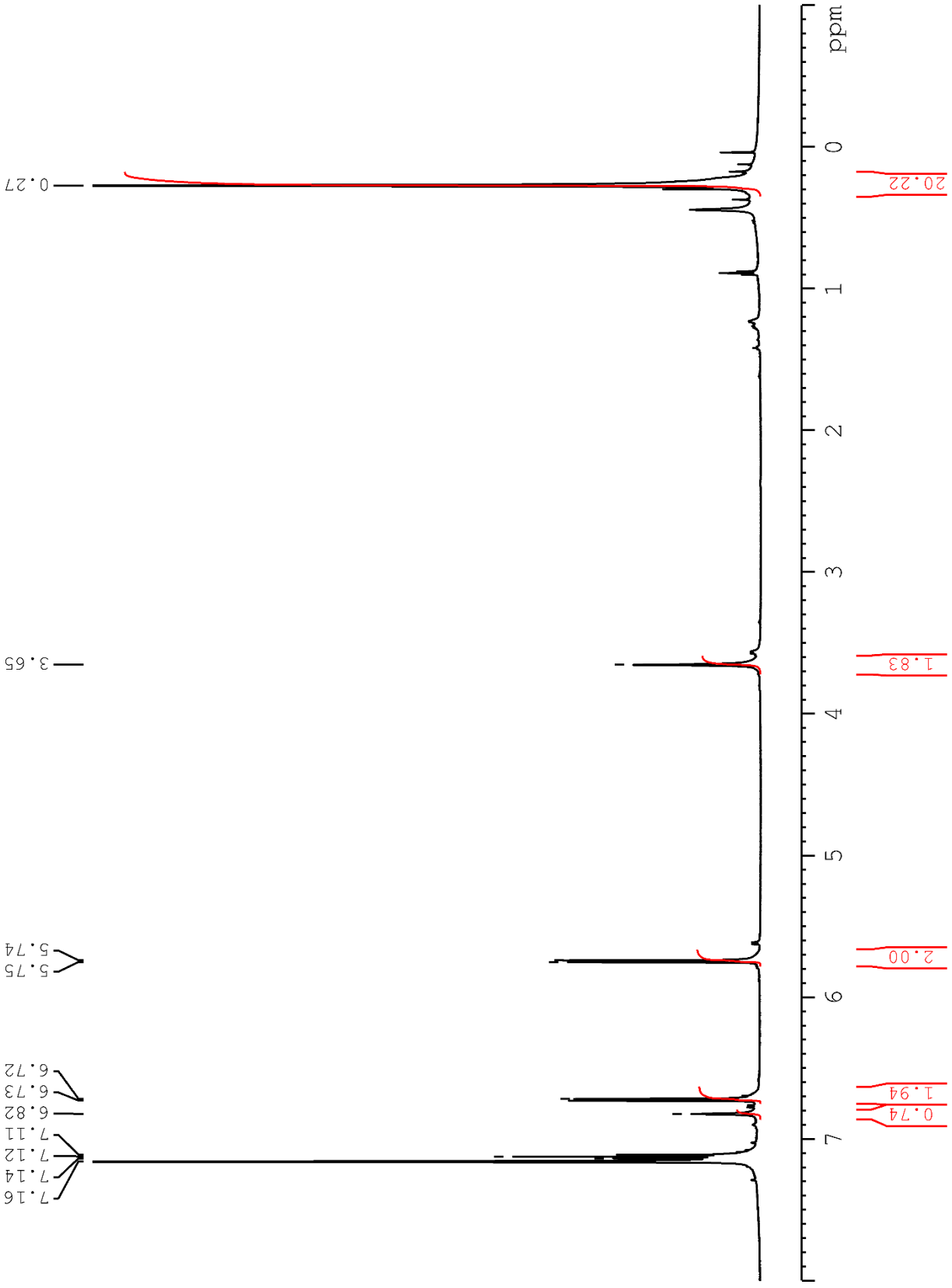

Figure S7. ^{1}H NMR spectrum of H_3L in C_6D_6 (600.13 MHz) at 298 K.

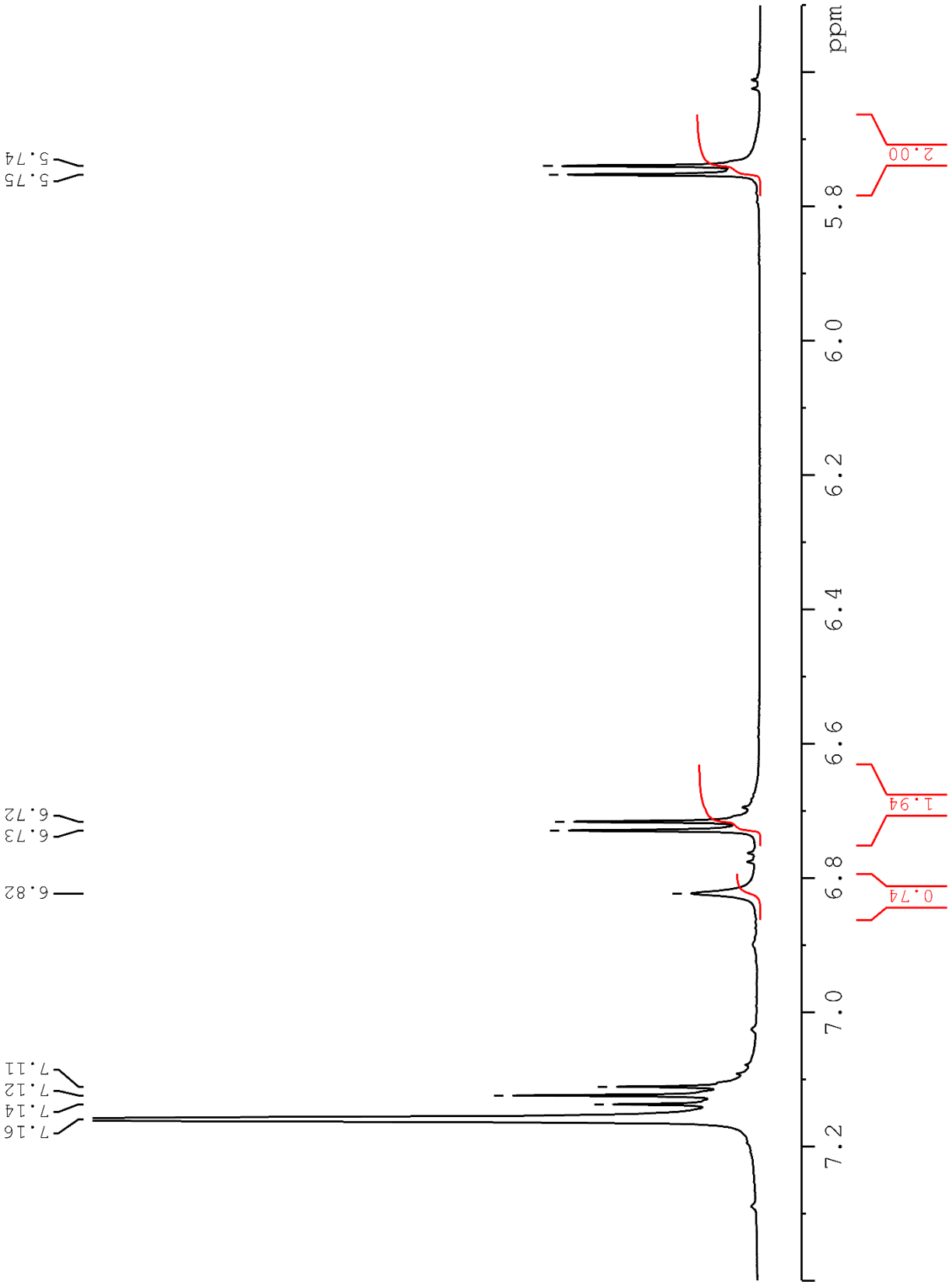

Figure S8. ^{1}H NMR spectrum of H_3L in C_6D_6 (600.13 MHz) at 298 K (expanded region).

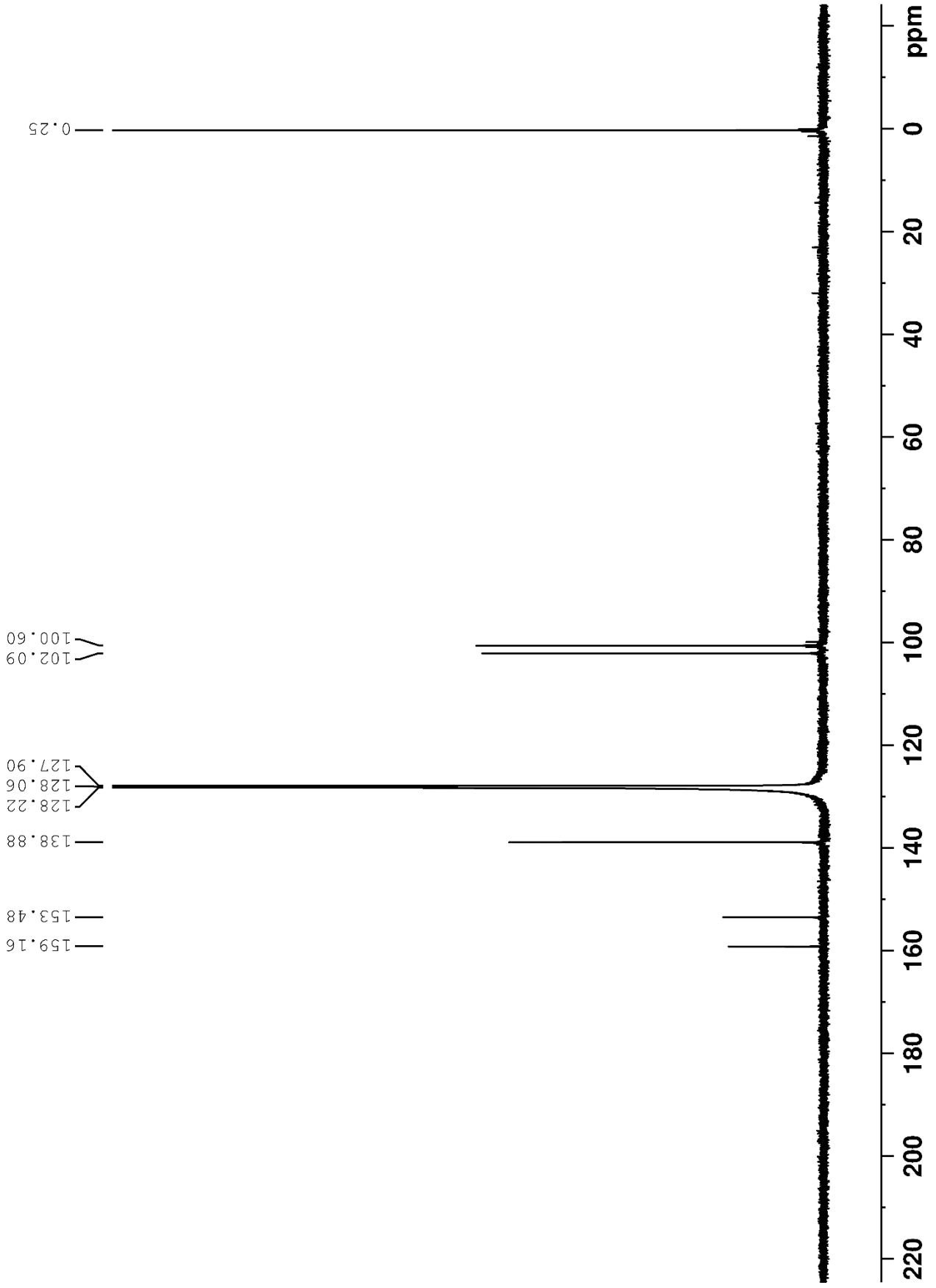

Figure S9. ^{13}C NMR spectrum of H_3L in C_6D_6 (150.90 MHz) at 298 K.

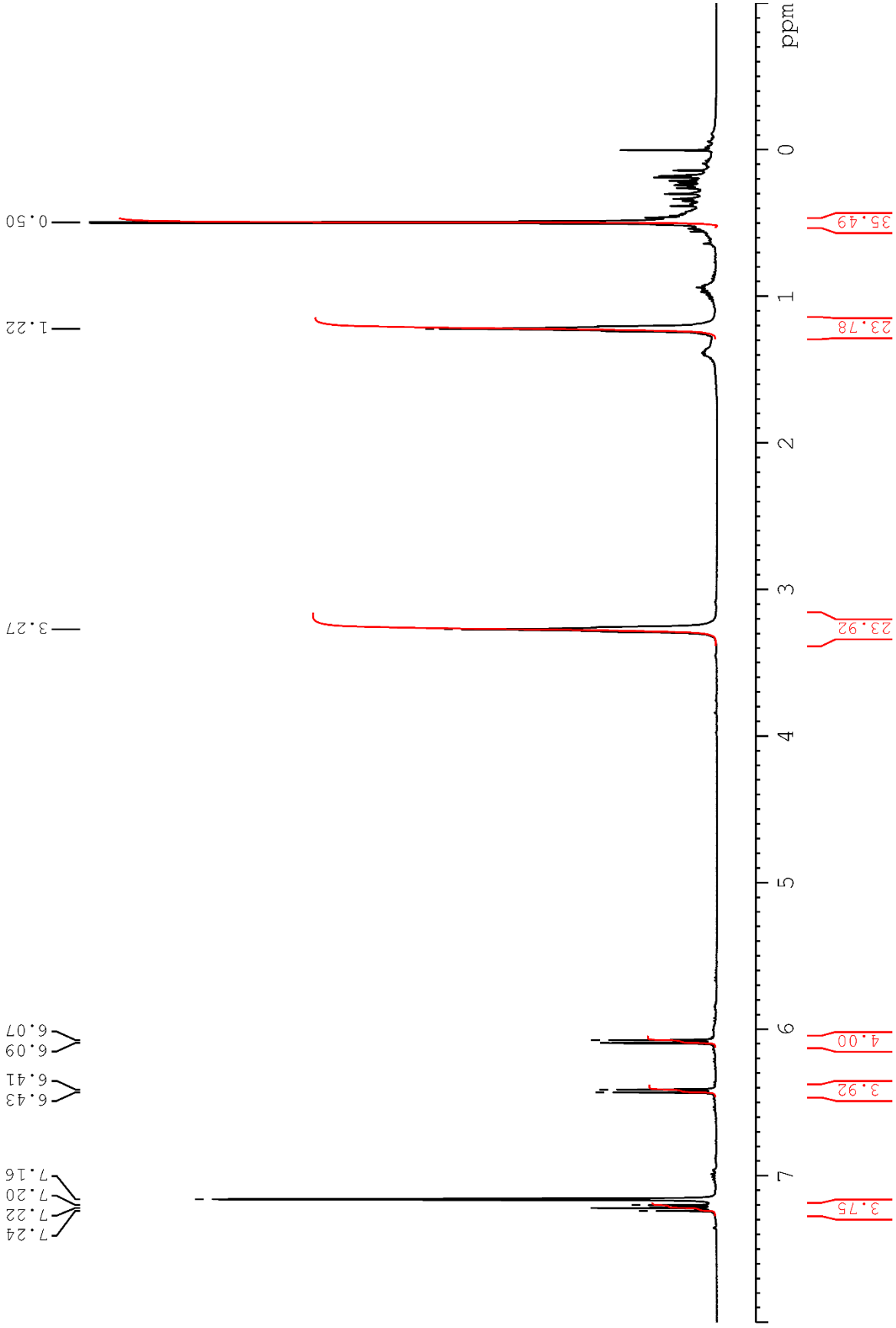

Figure S10. ^{1}H NMR spectrum of crude **1** in C_6D_6 (400.13 MHz) at 298 K. δ = 0.50 (s, 36H, $(CH_3)_3Si$), 1.22 (m, 24H, $CH_2CH_2O_{thf}$), 3.27 (m, 24H, CH_2O_{thf}), 6.08 (d, $^{3}J_{H\text{-}H}$ = 8.0 Hz, 4H, H^5), 6.42 (d, $^{3}J_{H\text{-}H}$ = 7.8 Hz, 4H, H^3), 7.22 ppm (t, $^{3}J_{H\text{-}H}$ = 8.2 Hz, 4H, H^4).

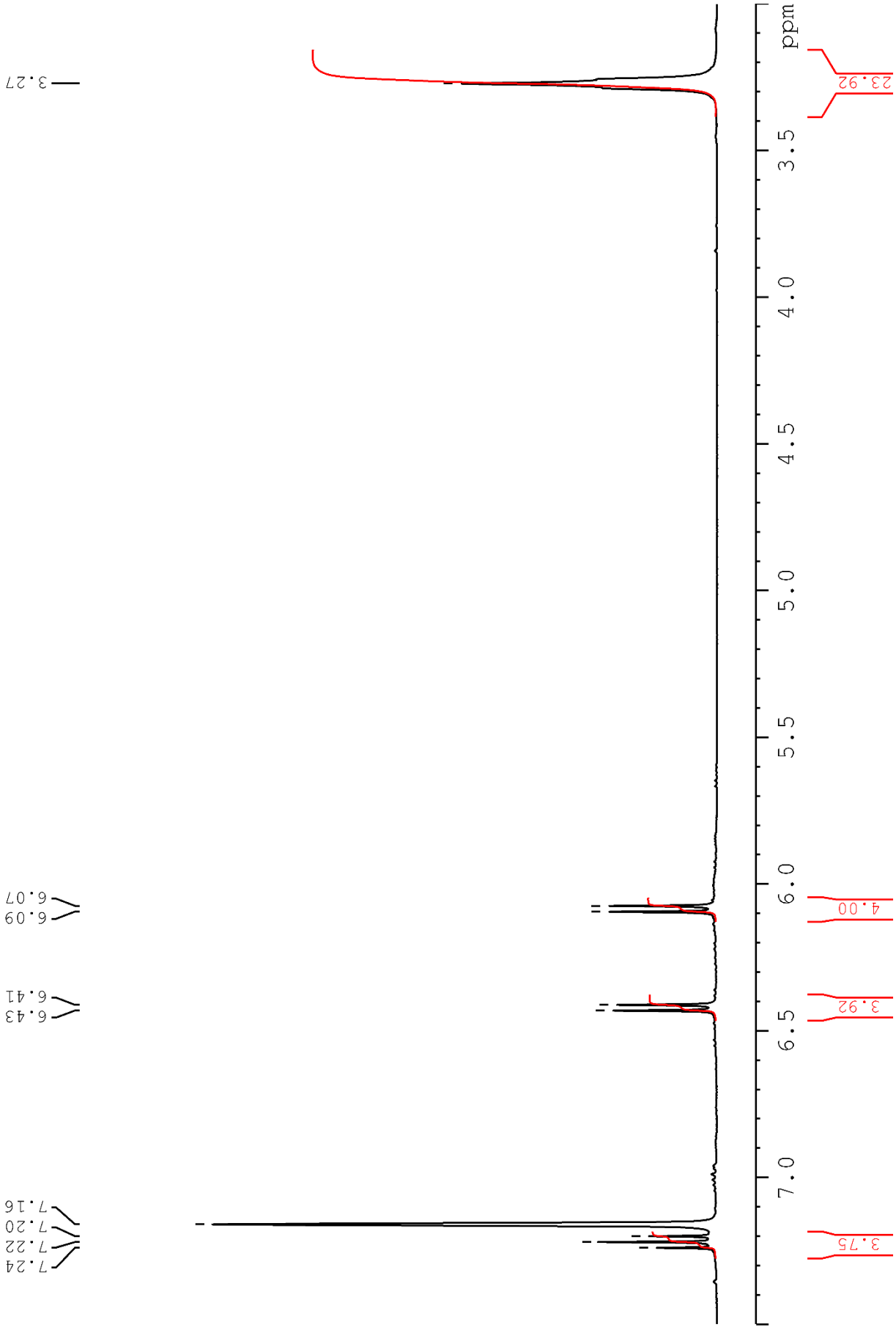

Figure S11. ^{1}H NMR spectrum of crude **1** in C_6D_6 (400.13 MHz) at 298 K (expanded region).

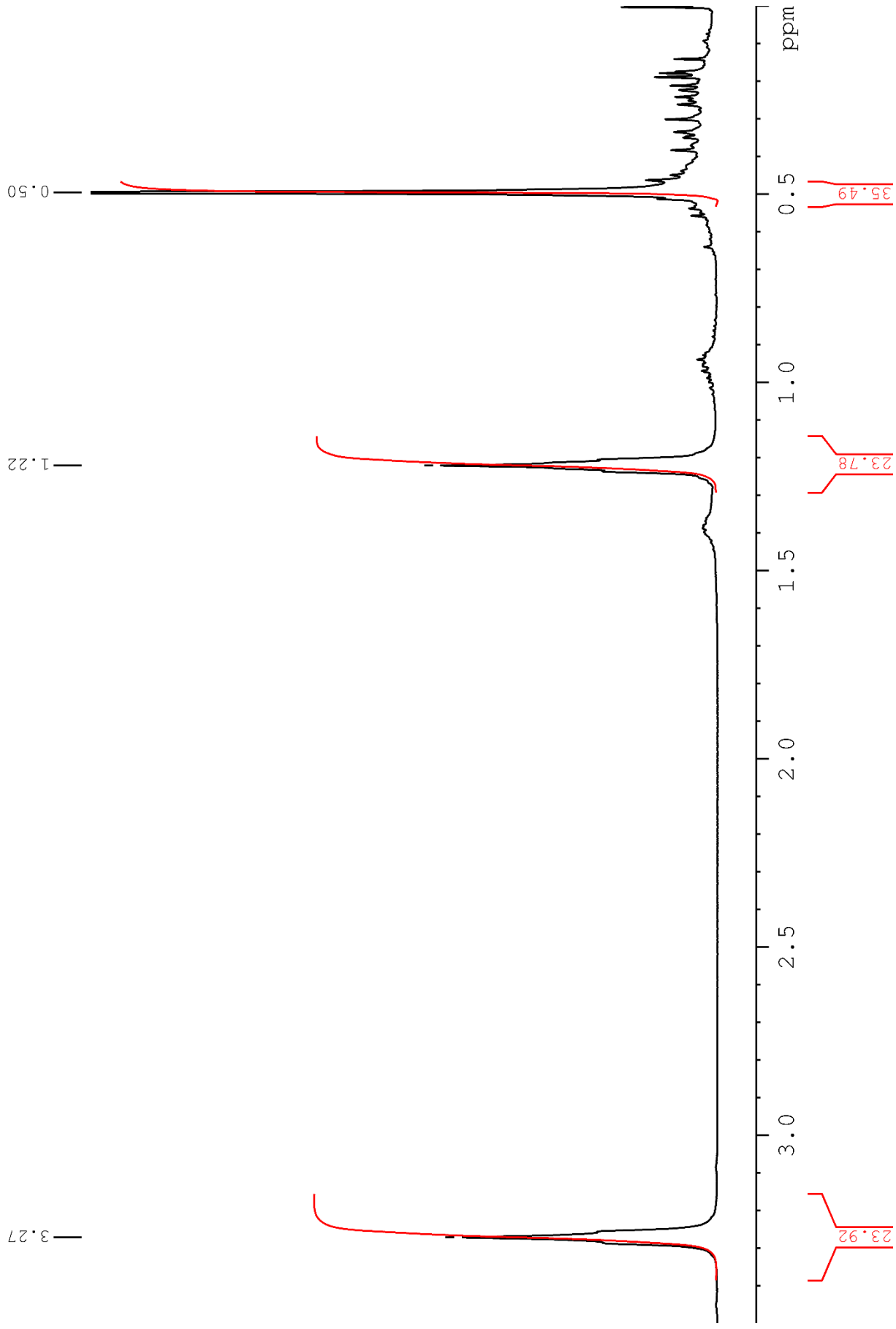

Figure S12. ^{1}H NMR spectrum of crude **1** in C_6D_6 (400.13 MHz) at 298 K (expanded region).

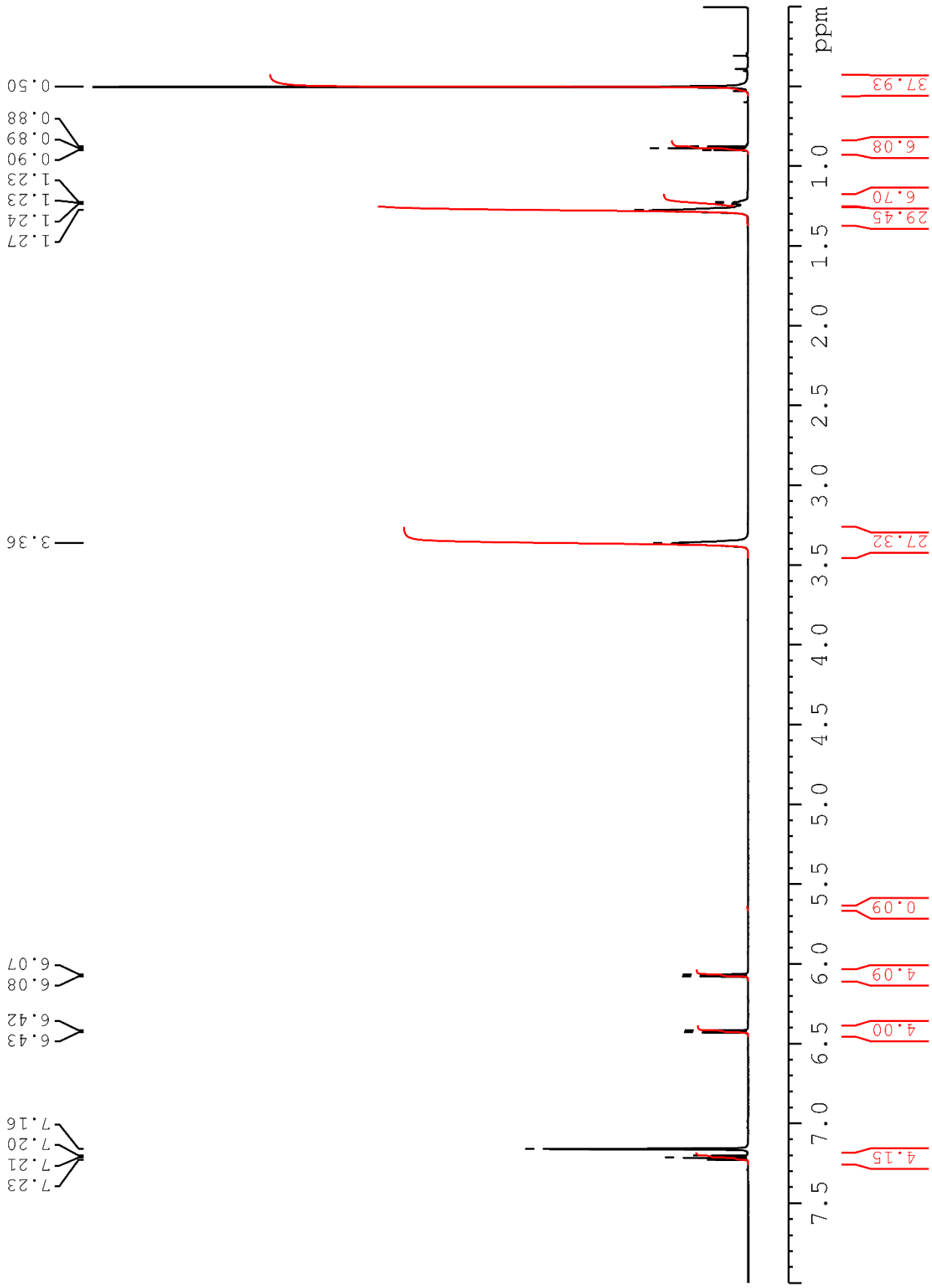

Figure S13. ^{1}H NMR spectrum of **1**·C_6H_{14} in C_6D_6 (600.13 MHz) at 298 K.

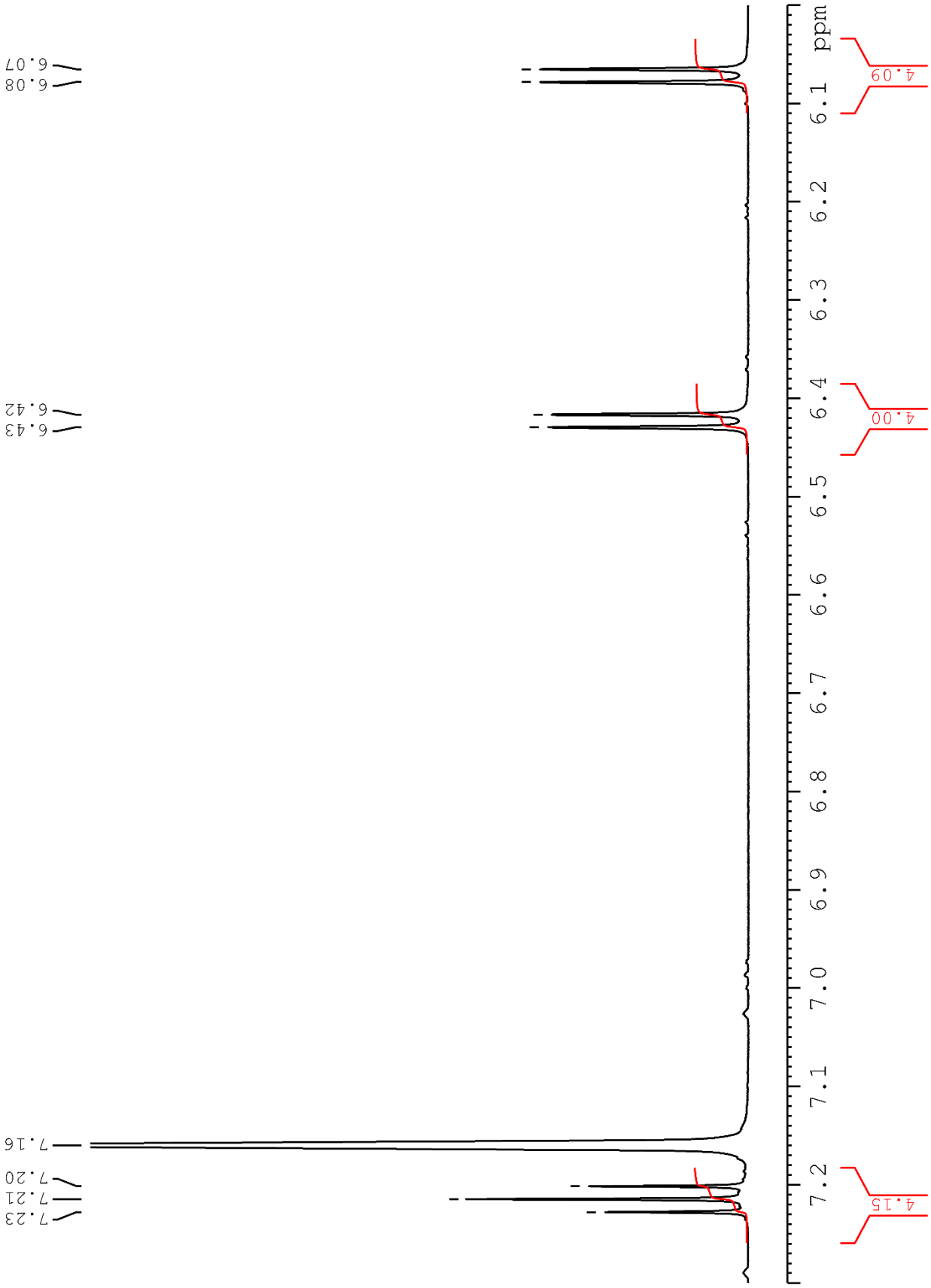

Figure S14. ^{1}H NMR spectrum of **1**·C_6H_{14} in C_6D_6 (600.13 MHz) at 298 K (expanded region).

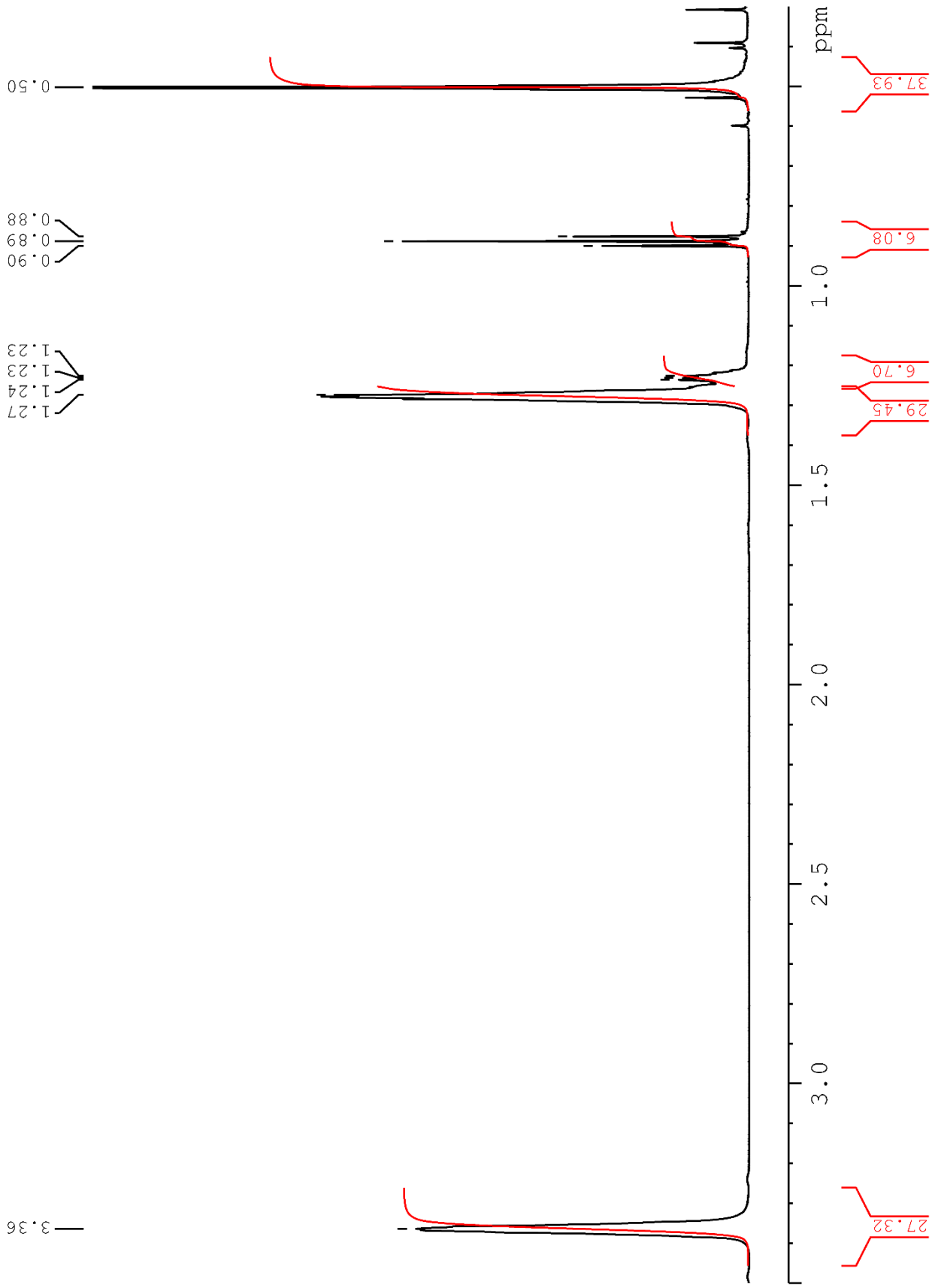

Figure S15. ^{1}H NMR spectrum of **1**·C_6H_{14} in C_6D_6 (600.13 MHz) at 298 K (expanded region).

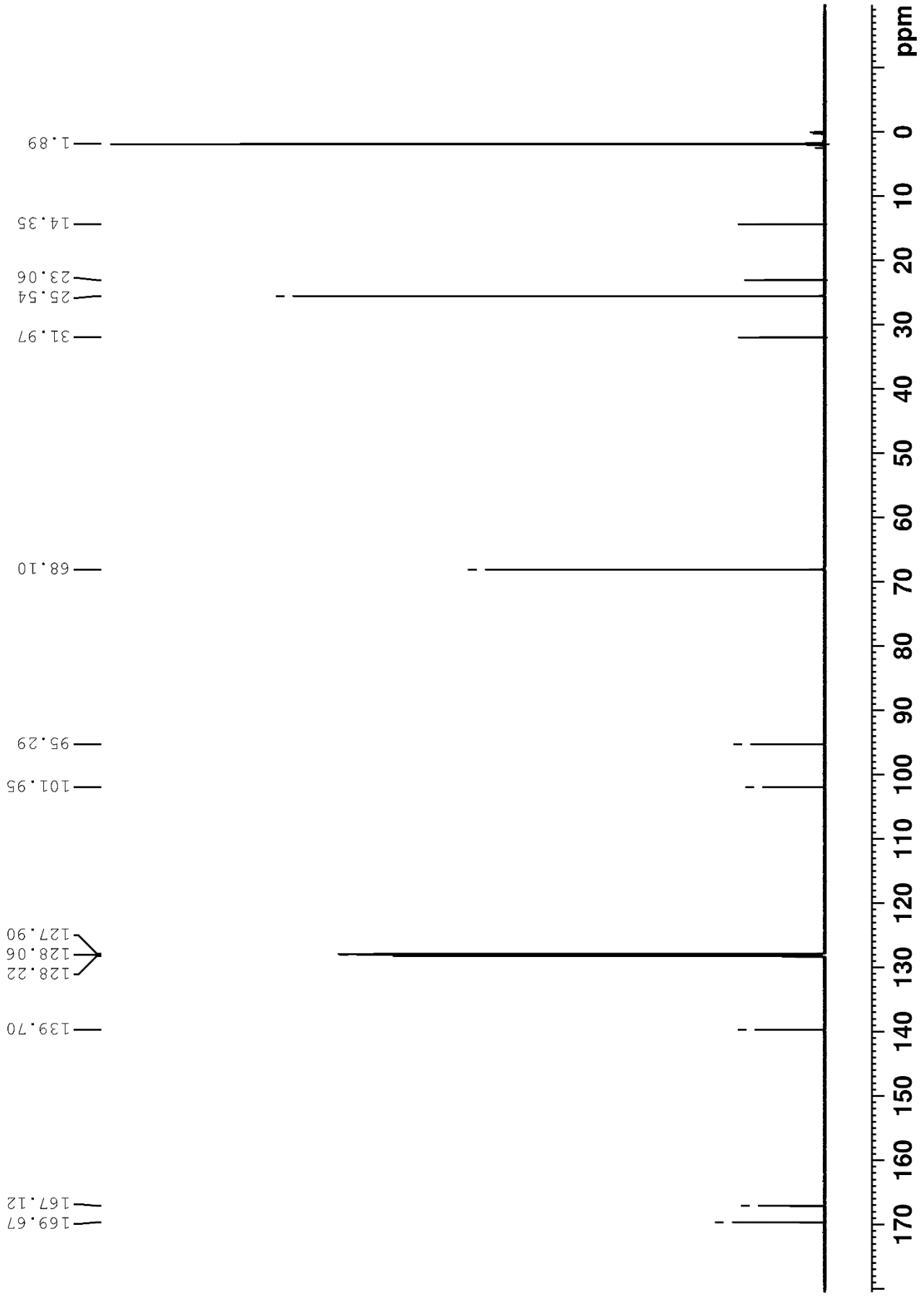

Figure S16. ^{13}C NMR spectrum of **1**·C_6H_{14} in C_6D_6 (150.90 MHz) at 298 K.

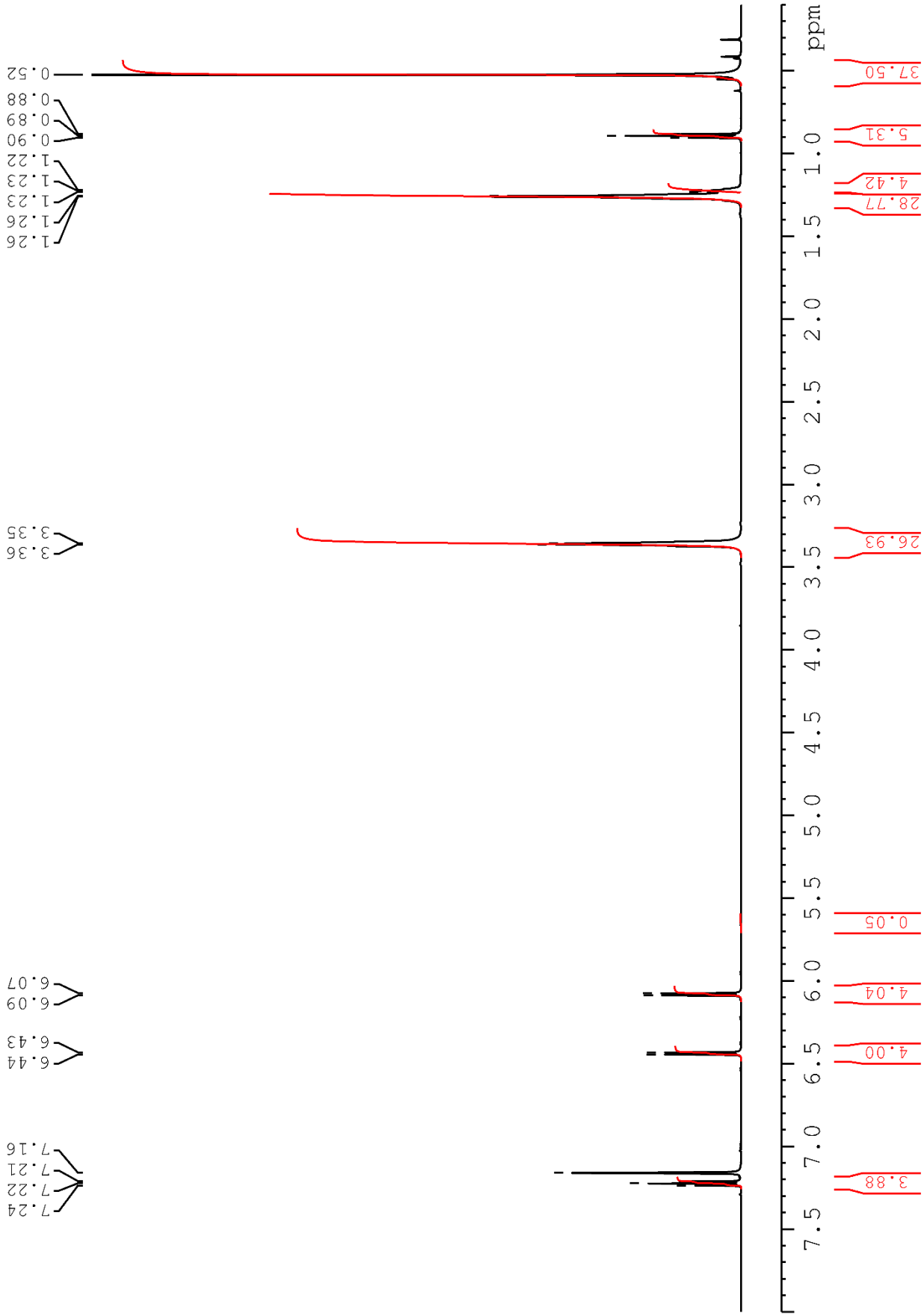

Figure S17. ^{1}H NMR spectrum of **1**·C_6H_{14} in C_6D_6 (600.13 MHz) at 283 K.

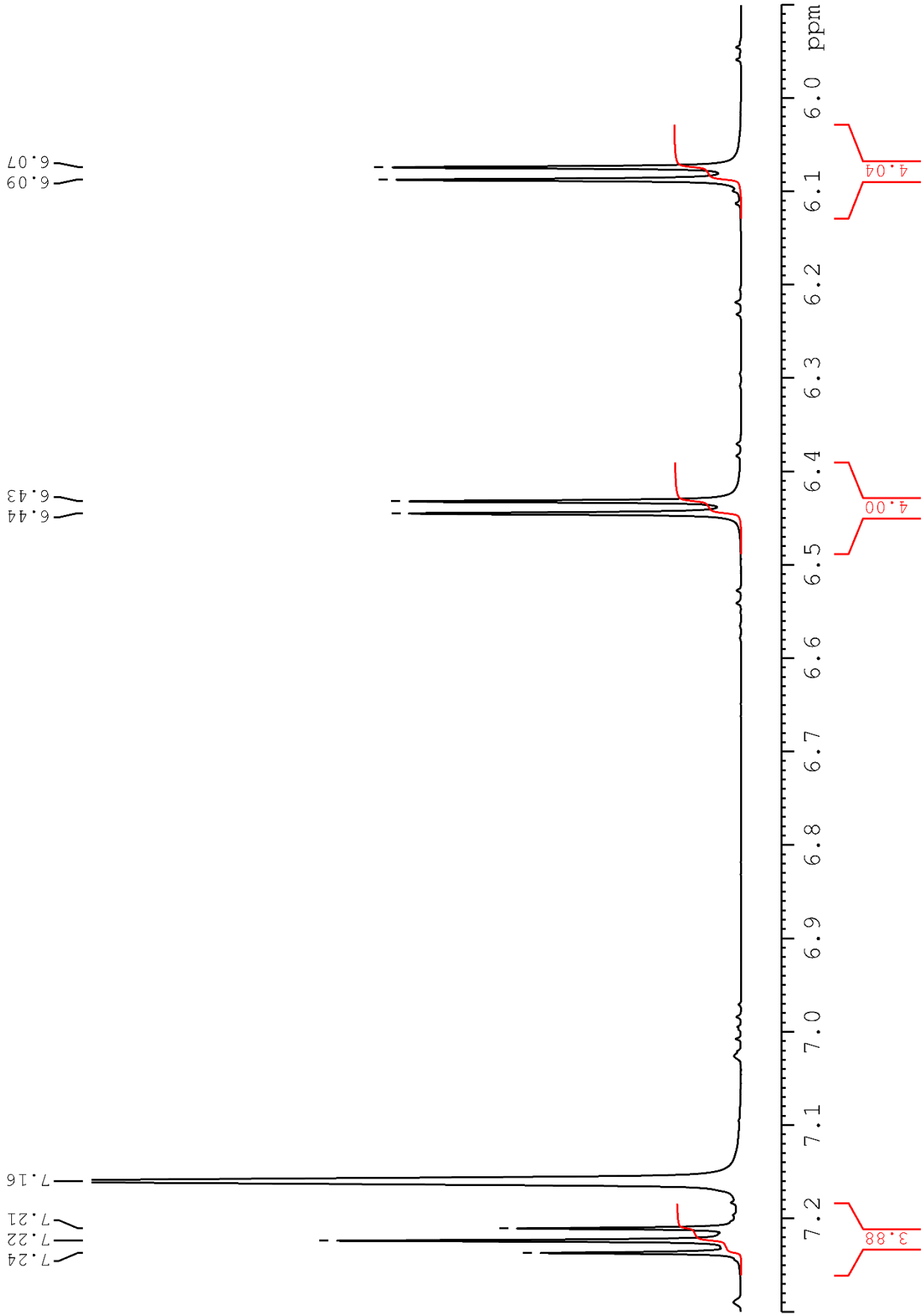

Figure S18. ^{1}H NMR spectrum of **1**·C_6H_{14} in C_6D_6 (600.13 MHz) at 283 K (expanded region).

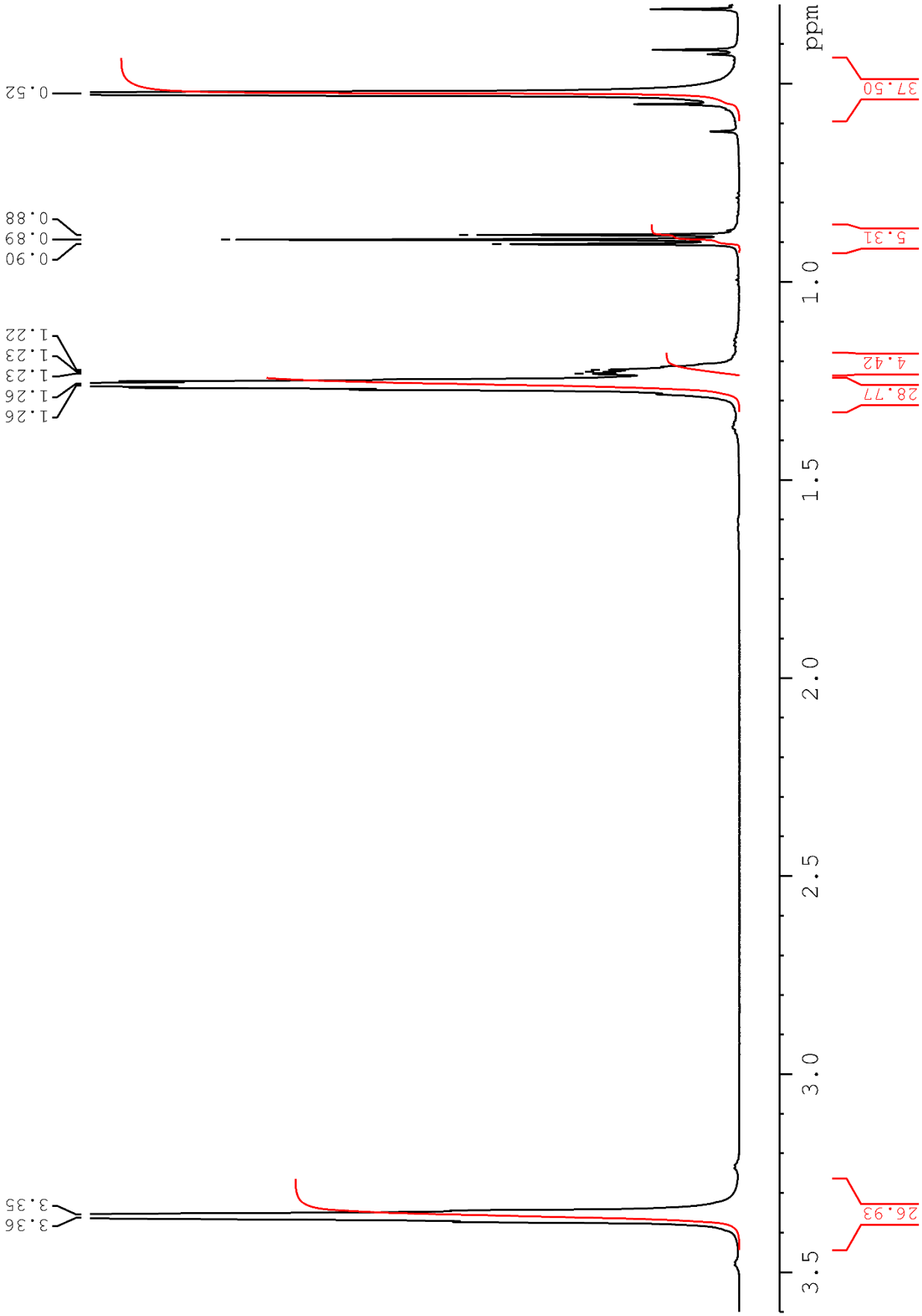

Figure S19. ^{1}H NMR spectrum of **1**·C_6H_{14} in C_6D_6 (600.13 MHz) at 283 K (expanded region).

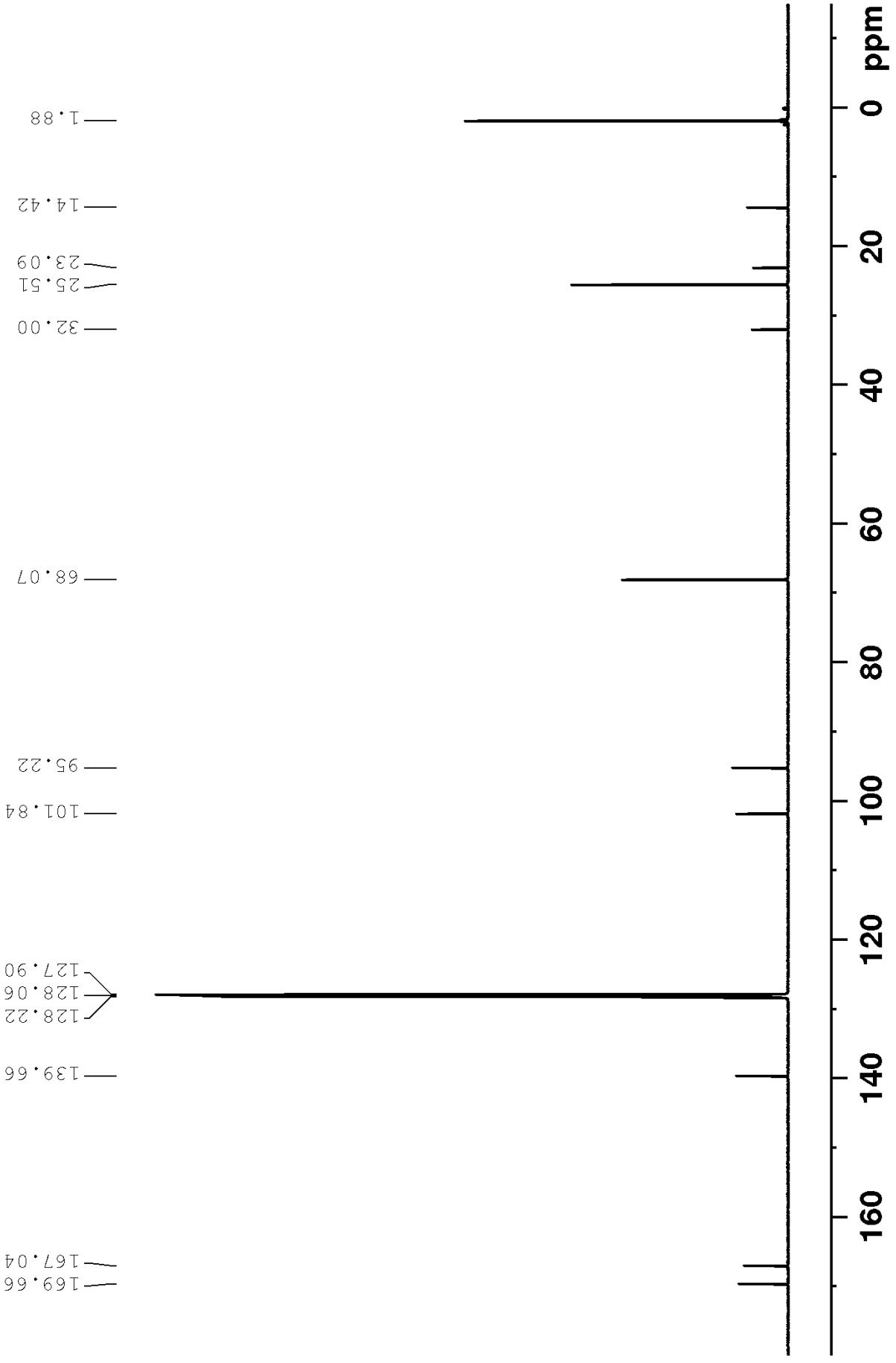

Figure S20. ^{13}C NMR spectrum of **1**·C_6H_{14} in C_6D_6 (150.90 MHz) at 283 K.

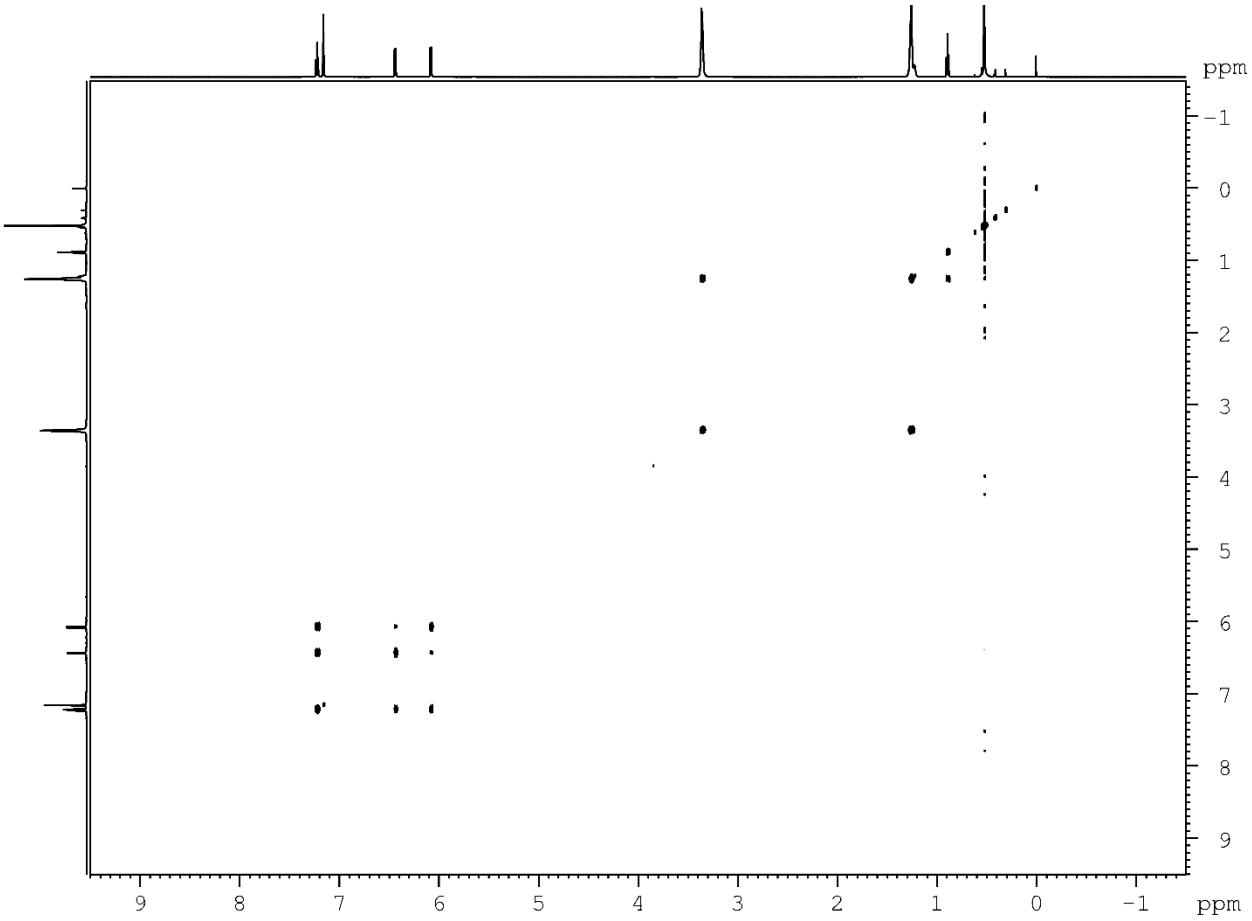

Figure S21. ^{1}H-^{1}H COSY spectrum of **1**·C_6H_{14} in C_6D_6 at 283 K.

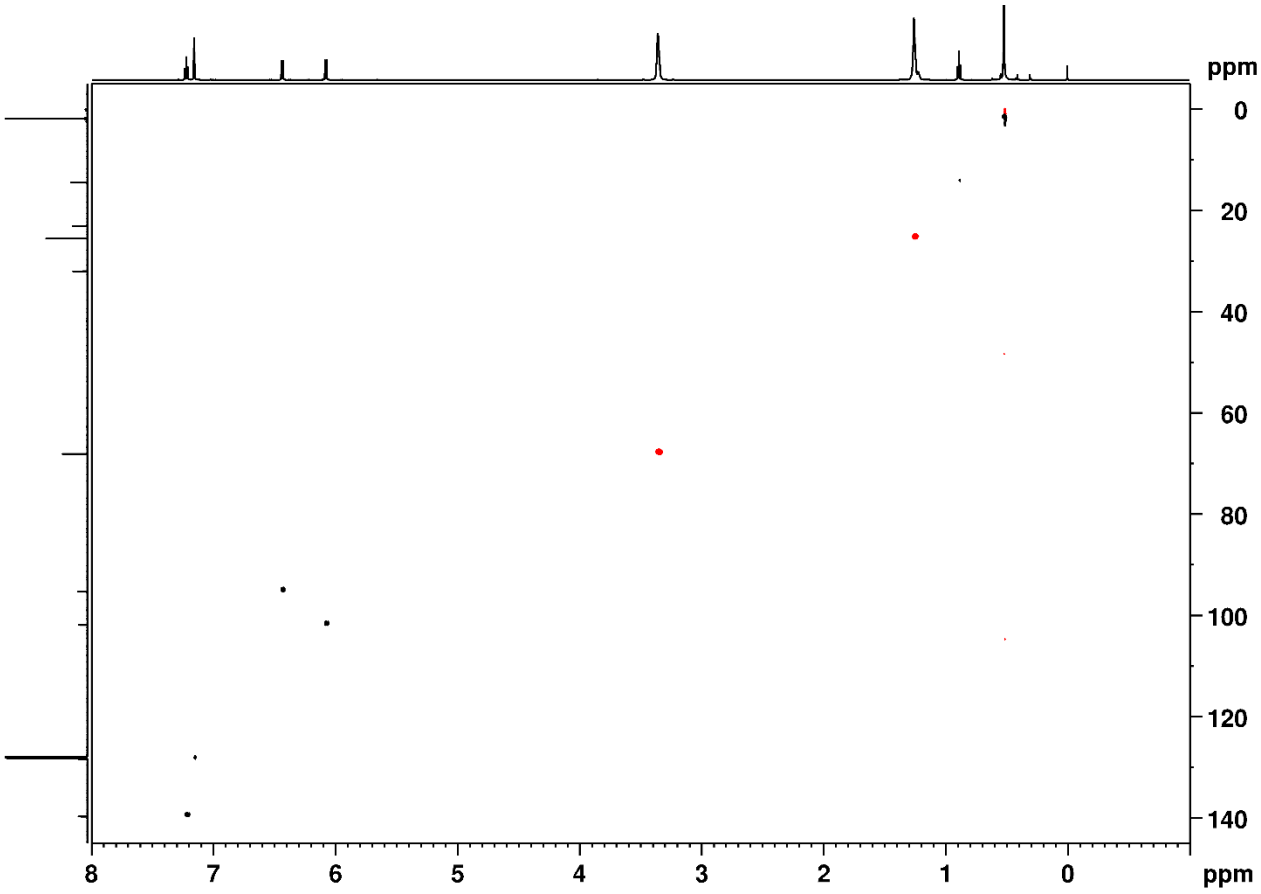

Figure S22. ^{1}H-^{13}C HSQCed spectrum of **1**·C_6H_{14} in C_6D_6 at 283 K.

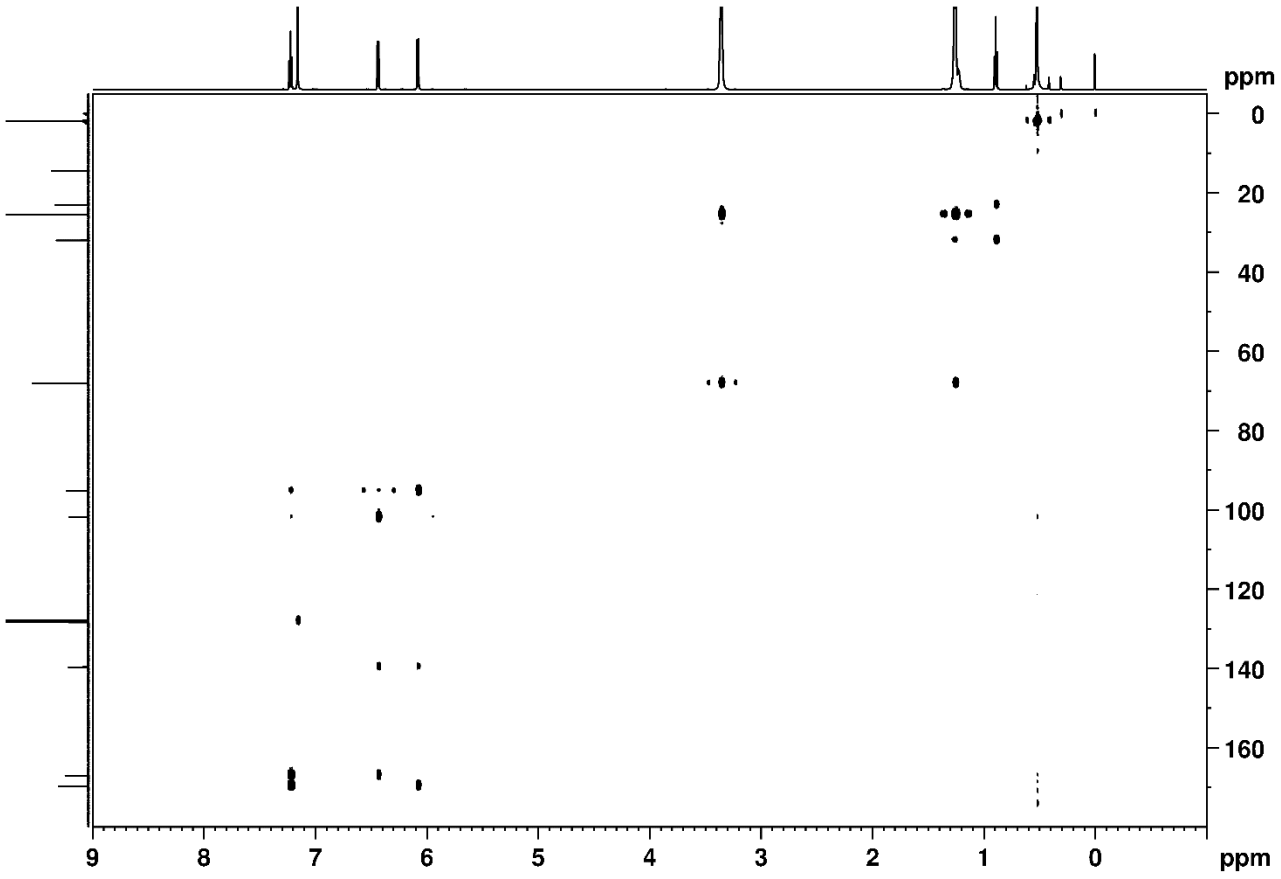

Figure S23. ^{1}H-^{13}C HMBC spectrum of **1**·C_6H_{14} in C_6D_6 at 283 K.

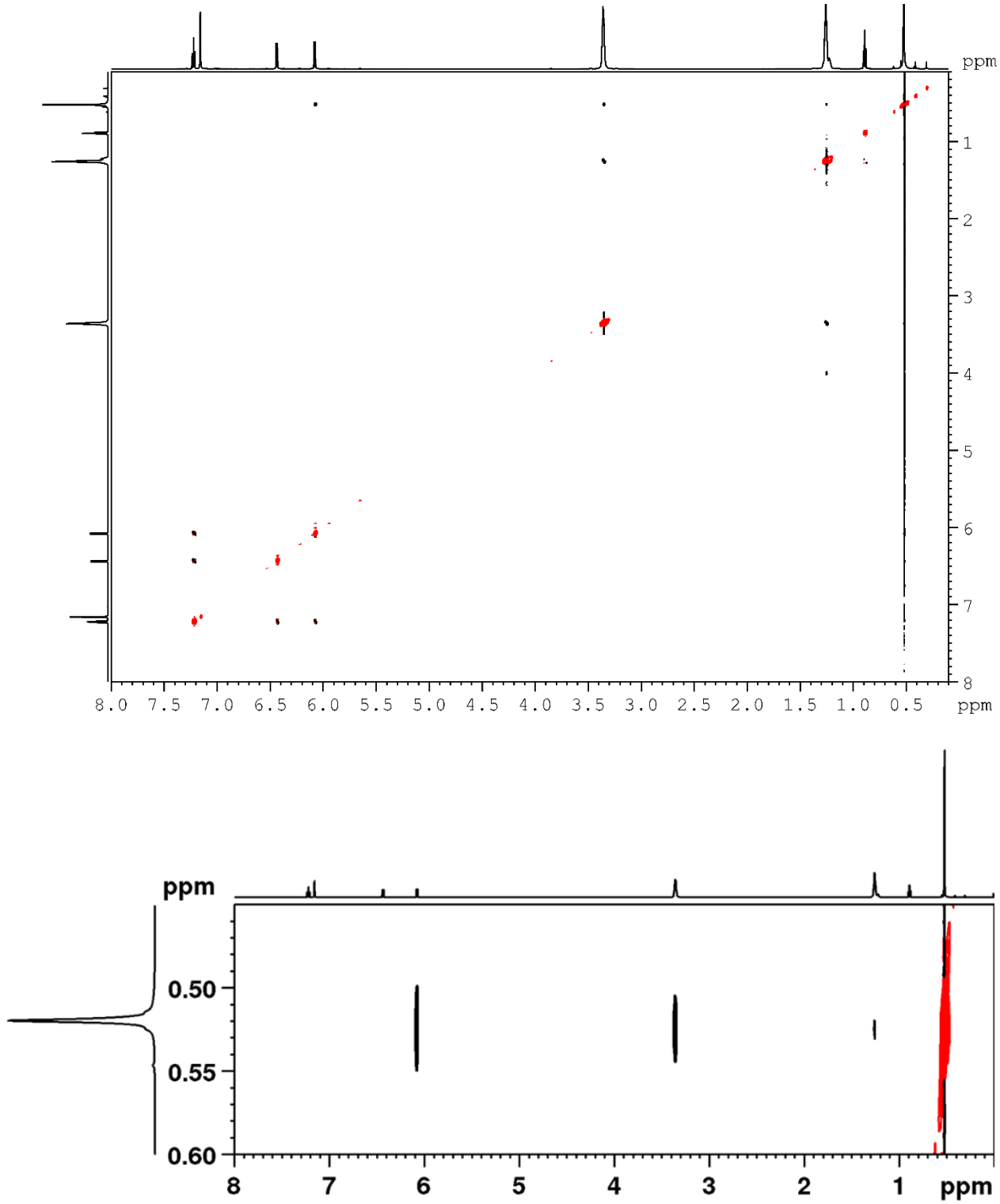

Figure S24. ^{1}H-^{1}H ROESY spectrum of **1**·C_6H_{14} in C_6D_6 at 283 K. The lower panel shows the cross peaks of $(CH_3)_3Si$ with H^5, CH_2O_{thf}, and $CH_2CH_2O_{thf}$.

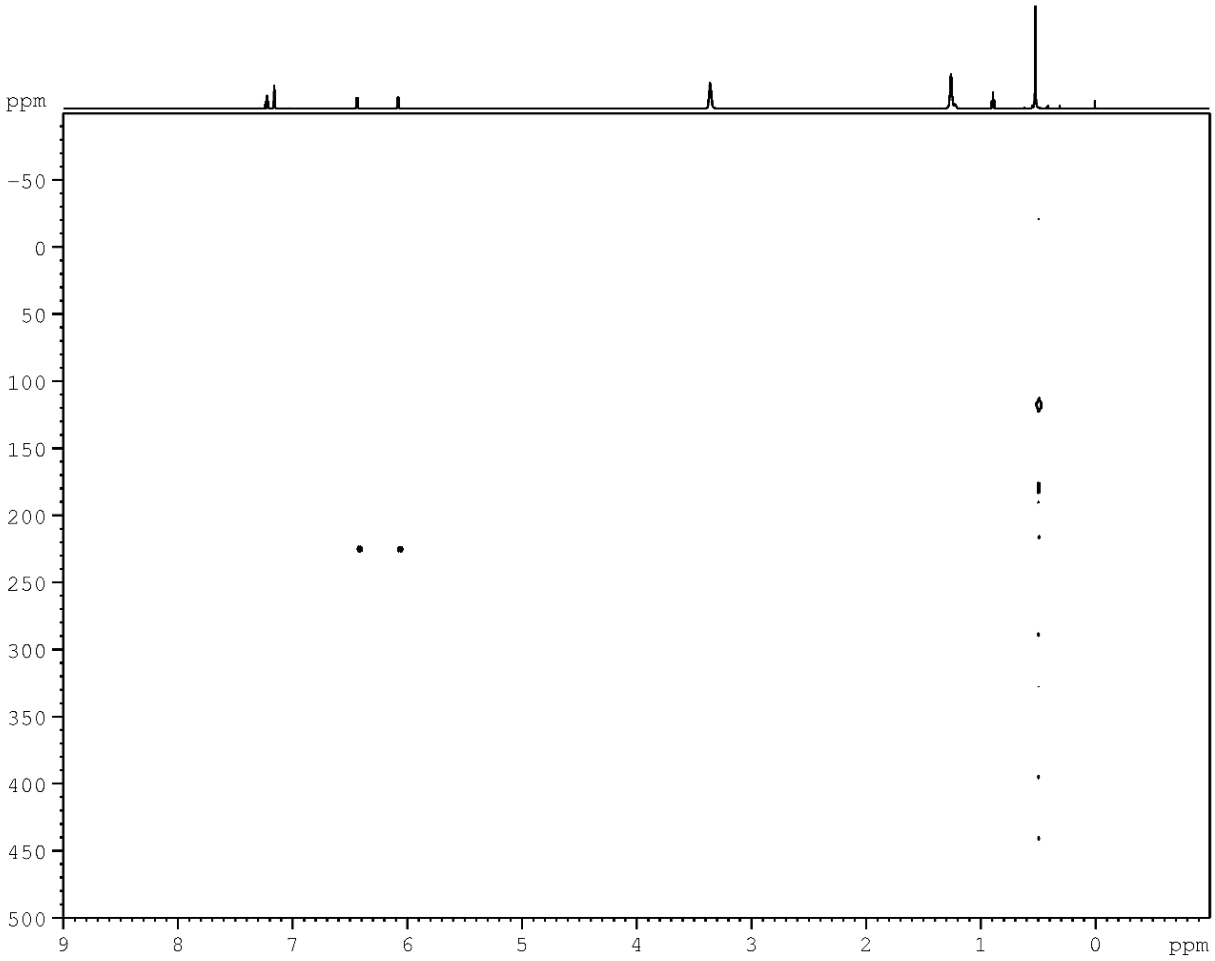

Figure S25. ^{1}H-^{15}N HMBC spectrum of **1**·C_6H_{14} in C_6D_6 at 283 K.

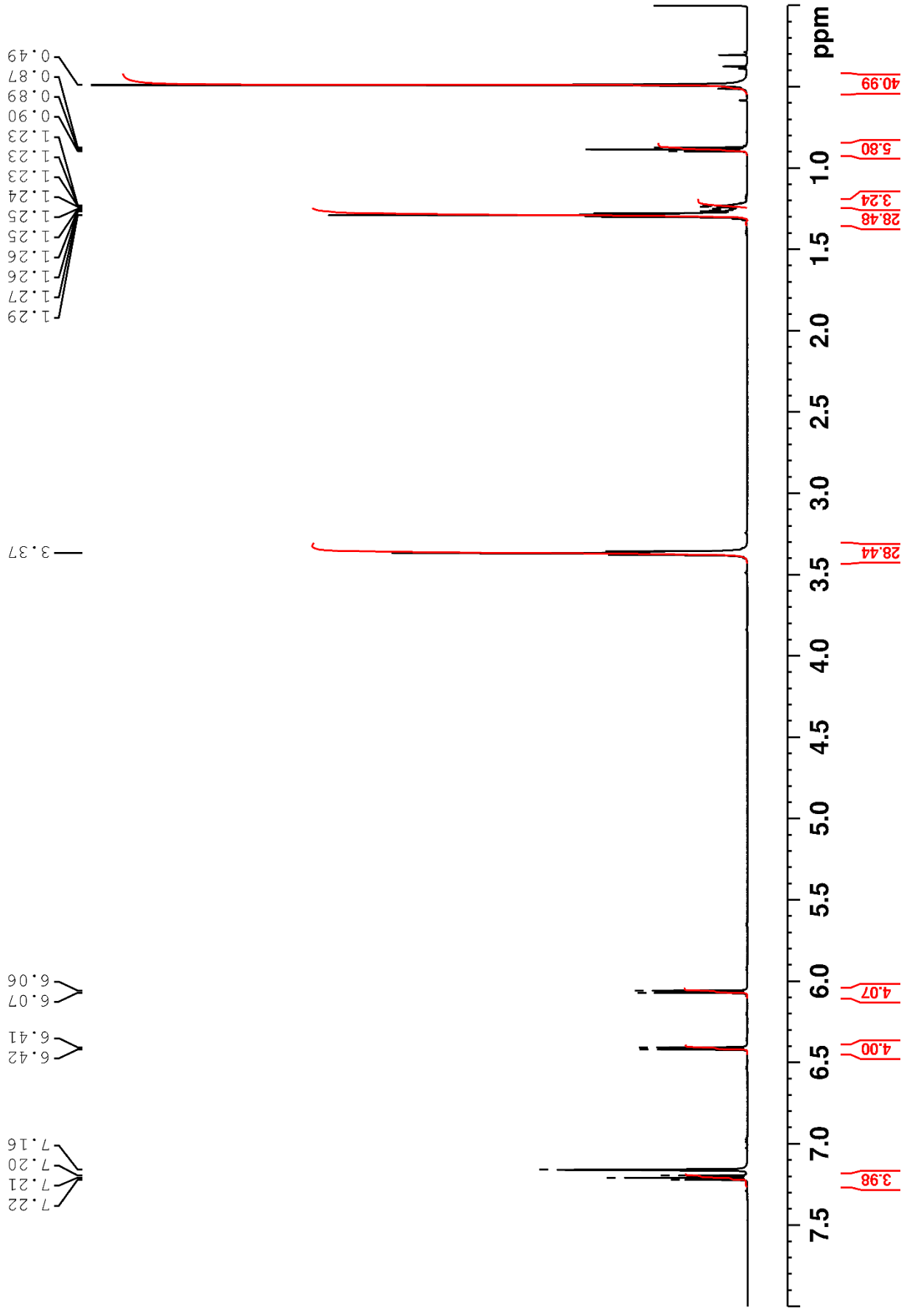

Figure S26. ^{1}H NMR spectrum of **1**·C_6H_{14} in C_6D_6 (600.13 MHz) at 310 K.

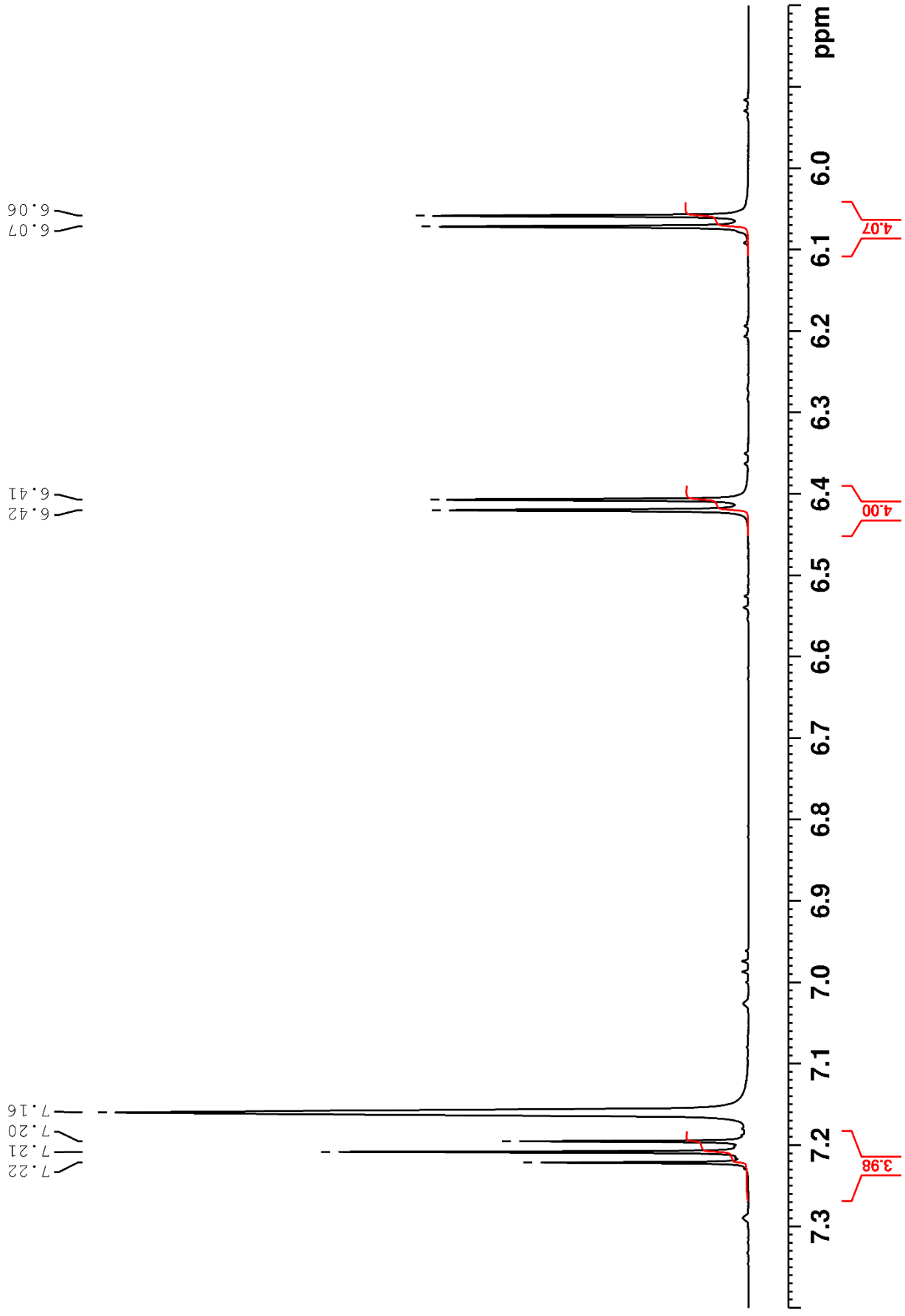

Figure S27. ^{1}H NMR spectrum of **1**·C_6H_{14} in C_6D_6 (600.13 MHz) at 310 K (expanded region).

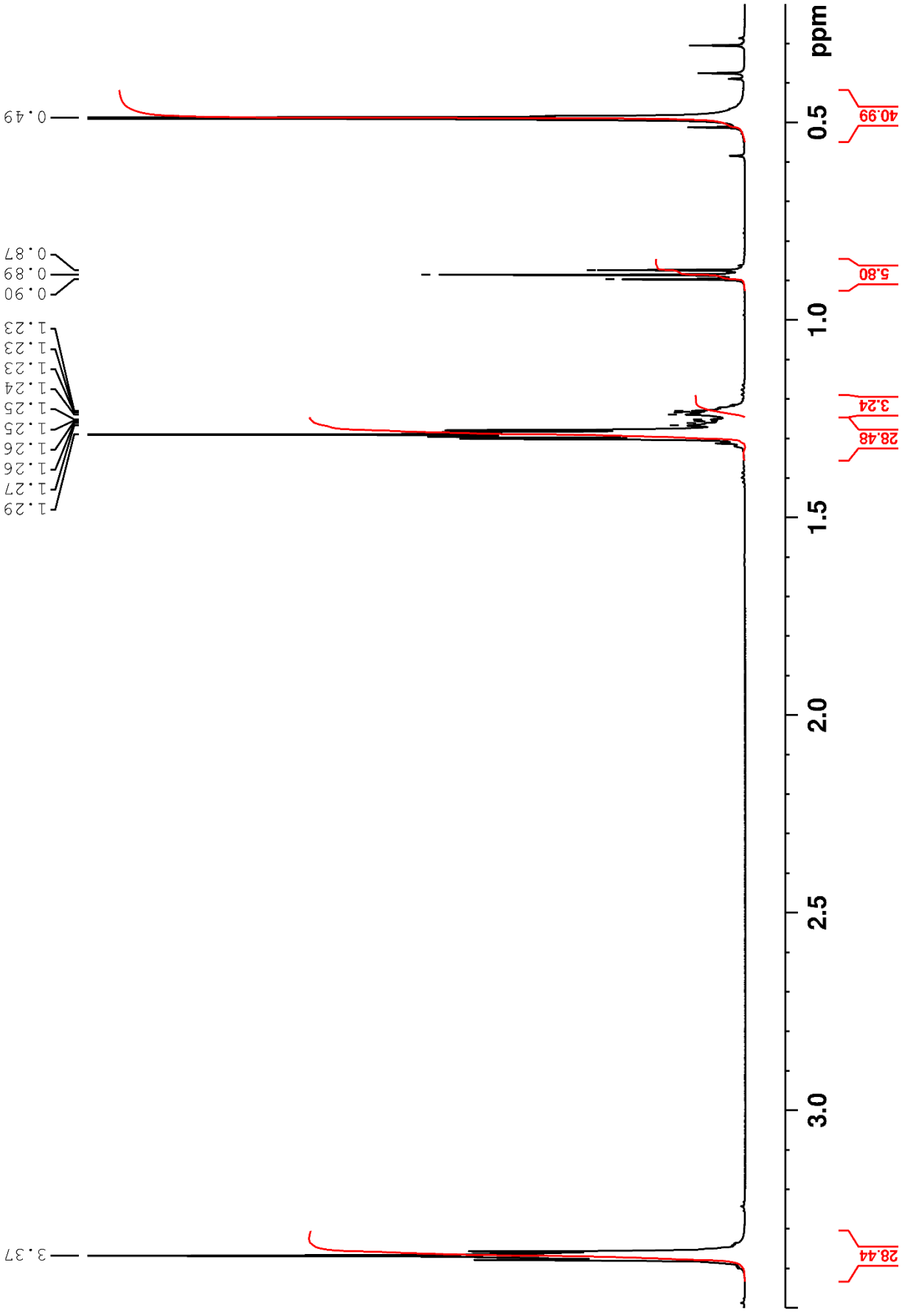

Figure S28. ^{1}H NMR spectrum of **1**·C_6H_{14} in C_6D_6 (600.13 MHz) at 310 K (expanded region).

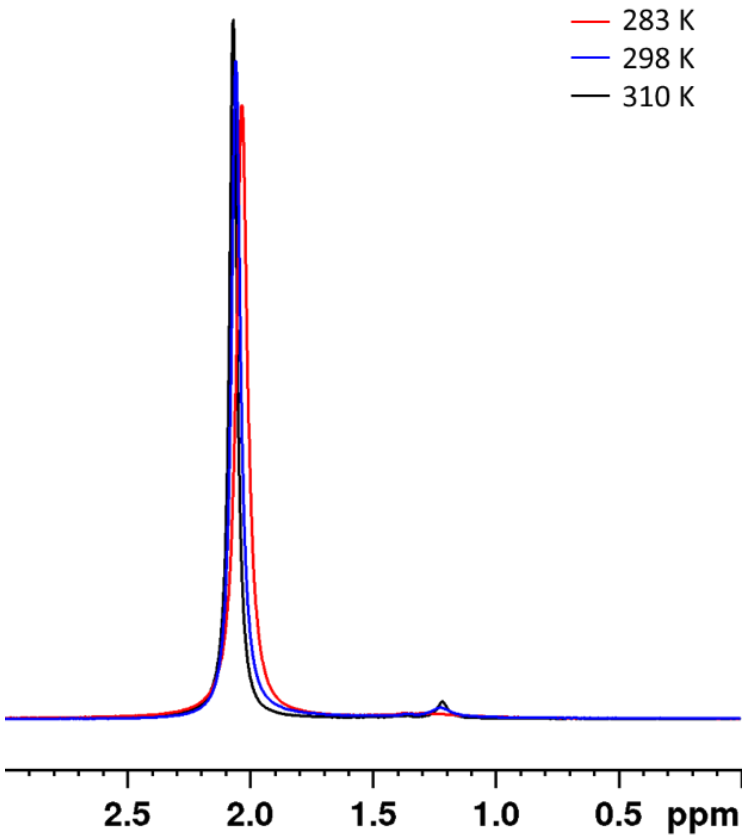

Figure S29. ^{7}Li NMR spectrum of **1**·C_6H_{14} in C_6D_6 (233.23 MHz) at three different temperatures. Chemical shift values for majority (minority) signals are 2.03 (1.29) ppm at 283 K, 2.06 (1.22) ppm at 298 K, and 2.07 (1.22) ppm at 310 K.

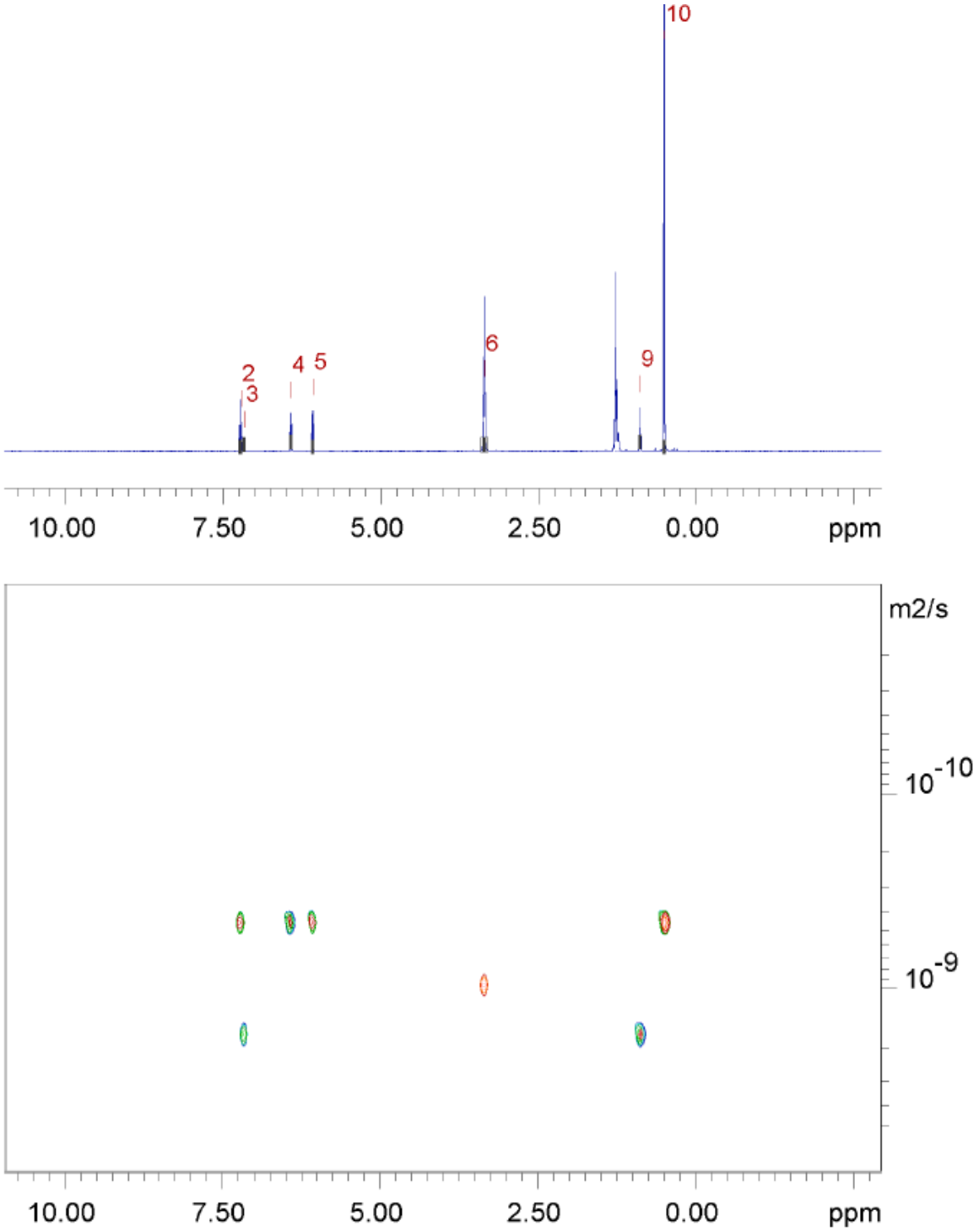

Figure S30. ^{1}H DOSY spectrum of **1** in C_6D_6 (400.13 MHz) at 298 K. The CH_2CH_2O signal of thf was not fitted as it extensively overlaps with peaks from *n*-hexane.

Table S1. Crystal data and refinement parameters for β-H_5A, **1**·C_6H_{14}, and **2**.

Compound	β-H_5A	**1**·C_6H_{14}	**2**
Formula	$C_{10}H_{11}N_5$	$C_{62}H_{110}Li_6N_{10}O_6Si_4$	$C_{48}H_{80}Li_6N_{10}O_4Si_4$
Molar mass (g mol^{-1})	201.24	1245.59	1015.22
T (K)	298(2)	115(2)	115(2)
Crystal system	monoclinic	orthorhombic	triclinic
Space group	*Cc*	*Pbcn*	$P\bar{1}$
a (Å)	22.7654(8)	17.5998(6)	13.9508(10)
b (Å)	5.1397(2)	22.9506(7)	19.1445(14)
c (Å)	16.9153(7)	18.4039(6)	23.3537(14)
α (°)	90.000	90	74.091(2)
β (°)	104.211(2)	90	74.507(2)
γ (°)	90.000	90	84.158(3)
V (Å^3)	1918.65(13)	7433.8(4)	5777.7(7)
Z	8	4	4
ρ_{calcd} (g cm^{-3})	1.393	1.113	1.167
μ (mm^{-1})	0.092	0.131	0.151
Crystal size (mm^3)	0.62×0.078×0.034	0.55×0.22×0.18	0.31×0.20×0.08
θ_{max} (°)	27.510	28.633	26.062
Number of reflections collected	10058	68236	95811
Number of independent reflections	3988	9434	22537
R_{int}	0.0255	0.0390	0.0525
Parameters/constraints	303/2	463/88	1371/144
$R1$, $wR2$	0.0580, 0.0823	0.0705, 0.1473	0.0914, 0.1227
$R1$, $wR2$ [$I > 2\sigma(I)$]	0.0369, 0.0746	0.0466, 0.1333	0.0449, 0.1055
GOF	1.014	1.067	1.052
Residues max/min (eÅ^{-3})	0.121/–0.184	0.497/–0.483	0.490/–0.342
Radiation used (Å)	0.71073 (Mo-Kα)	0.71073 (Mo-Kα)	0.71073 (Mo-Kα)

Table S2. Assignment of ^{1}H and ^{13}C NMR signals for **1**·C_6H_{14} in C_6D_6 at 283 K.

δ_H (ppm)	multiplicity	integrated intensity	$^{3}J_{H\text{-}H}$ (Hz)	δ_C (ppm)	Assignment
7.22	t	4H	7.9	**139.66**	H^4/C^4
6.44	d	4H	7.8	**95.22**	H^3/C^3
6.08	d	4H	7.9	**101.84**	H^5/C^5
0.52	s	36H	/	**1.88**	$(CH_3)_3Si$ $^{1}J_{C\text{-}Si}$ = 54.3 Hz $^{2}J_{H\text{-}Si}$ = 6.2 Hz
/	/	/	/	**167.04**	C^2
/	/	/	/	**169.66**	C^6
1.25	m	24H	/	**25.51**	CH_2CH_2O thf
3.36	m	24H	/	**68.07**	CH_2O thf
0.89	t	6H	/	**14.42**	CH_3 *n*-hexane
1.26	m	4H	/	**23.09**	CH_2CH_3 *n*-hexane
1.22	m	4H	/	**32.00**	$CH_2CH_2CH_3$ *n*-hexane

Table S3. Impurity NMR signals for **1**·C_6H_{14} in C_6D_6 at 283 K.[a]

δ_H (ppm)	multiplicity	integrated intensity	$^{3}J_{H\text{-}H}$ (Hz)	$\delta_{C/N}$ (ppm)[b]	Assignment	**ROE** correlations
7.18	t	1H	8.0	[c]	γ-H	
7.00	t	1H	7.8	139.8	γ'-H	
6.99	t	1H	8.0	140.0	γ''-H	
6.53	d	1H	8.2	99.8	β''a-H	3.36
6.37	d	1H	7.6	93.6	βa-H	3.36
6.22	d	1H	7.8	96.7	β'a-H	0.41 (weak)
6.10	d	1H	8.1	104.2	βb-H	0.55
5.95	d	1H	8.0	104.6	β'b-H	0.41
5.65	d	1H	7.8	95.0	β''b-H	0.31
3.84	s	1H	/	79	NH	0.31, 0.55 (weak)
0.55	s	9H	/	2.5	$(CH_3)_3Si$	
0.41	s	9H	/	1.9	$(CH_3)_3Si$	
0.31	s	9H	/	0.3	$(CH_3)_3Si$	

[a] In addition to one NH resonance, three sets of pyridyl and $(CH_3)_3Si$ signals are clearly distinguished; the fourth set is hidden by the ^{1}H NMR peaks of **1**. [b] ^{13}C and ^{15}N chemical shifts are obtained from HSQC and HMBC experiments, respectively. [c] Hidden by the H,C correlations of **1**.